University of Washington

Analysis of the Timing of Building Displacement during Intense Seismic Shaking for three Earthquakes, 2001 M_w 6.8 Nisqually (Washington State), 2017 M_w 7.1 Puebla (Mexico), 2018 M_w 7.1 2018 Anchorage (Alaska)

Nancy A. Sackman

MESSAGe Capstone Project, ESS 601A

Alison Duvall, Paul Bodin, Steven Walters

June 14, 2019

MESSAGe Technical Report Number 078

Executive Summary

Localized intense ground shaking from strong earthquakes pose significant hazards to humans including building damage that may lead to structural failure and possible collapse. Building failure can cause harm or loss of life and also result in economic loss. For example, in the 2017 M_w 7.1 Puebla Earthquake in Mexico, more than 300 people died with the majority of those deaths in Mexico City. More than 3000 buildings were damaged and 44 buildings collapsed (Grillo, 2017).

Structural engineers and designers study rigorously whether or not a building may experience damage and/or structural failure. However, little emphasis has been placed on the timing of displacement and/or failure during strong shaking. For example if a building were to fail late in a long-duration earthquake while the interstory drift rose to destructive levels, the advice to its occupants might be to attempt to evacuate.

Therefore, I undertook an analysis to explore factors that might impact and constrain the variability in timing to maximum building displacement. To provide a range of estimates of building response timing to shaking, I explored the buildings' temporal responses to different ground motions from seismic inputs recorded at different seismic stations. I modeled the building responses as a simple single degree of freedom oscillator, programmed in the Python programming language. I used ground motion recordings from three deep "intraslab" subduction zone earthquakes characterized by normal faulting, the 2001 Nisqually (Washington), the 2017 Puebla Earthquake, and the 2018 Anchorage Earthquake (Figures 1-3). Using computer simulations, I tested the responses of a range of concrete building heights from 1 to 30 stories tall.

Results show that the time to maximum building displacement changes with the height of a building and varies with distance to rupture as well as local site responses. While perhaps not an accurate indication of the absolute time when a building would fail, the time between the onset of an earthquake and the maximum displacement observed in the modeled building response can be interpreted as a proxy for time to failure and perhaps its relative sensitivity to seismic shaking.

Earthquake Early Warning (EEW) is a newly emerging technology that uses real-time seismic data, rapid telecommunications, and new real-time processing algorithms to provide several seconds to up to 3 minutes of advanced warning of strong shaking to an at risk population. The actual warning time depends on factors like the latency of the system and the distance the earthquake source is from the targeted at-risk population. Prior to EEW, the most efficient life saving action that disaster prevention officials could offer was, "when you feel shaking, drop, cover and hold on". With EEW, there is now the possibility of an additional response. Namely, if the timing of maximum building displacement from strong shaking were known for different storied buildings, it might be possible that warnings could be issued with sufficient lead time to allow people to exit the structure rather than shelter in place in a collapsing building. An EEW-mediated evacuation strategy would depend on the range of timing between an earthquake and a building collapse.

The single degree of freedom oscillator shows it can be a first step in quantifying the timing of building displacement during strong shaking. Understanding the tectonic setting, the distance of the rupture to an at-risk population, earthquake recurrence intervals, aftershock sequencing, earthquake directivity and seismic amplification should also be put into context when modeling earthquakes.

Table of Contents

Introduction

Earthquakes are one of the deadliest natural disasters in terms of loss of human life. From the year 2000 to 2015 over 50,000 people died annually on average worldwide from earthquakes (USGS, 2019). The main cause for earthquake fatalities are structural failure (Kenny, 2009) caused by the suddenness of displacement (Samuel and Weir, 2005). If people knew when strong shaking were to affect a building's maximum displacement, they may be able to take lifesaving action while inside a structure.

Earthquake early warning systems provide an alert and an estimate of when strong shaking is expected after an earthquake has been detected by a seismic network (Nakamura, 1988; Allen and Kanamori, 2003; Wu and Kanamori, 2008, Given et al., 2014). Early warning systems give out warnings to the public in several countries including China, Italy, Japan, Mexico, Romania, Taiwan, and Turkey. In the United States earthquake early warning, known as ShakeAlert, has been implemented in Los Angeles and is in test mode along the rest of the west coast. When a nearby fault ruptures, ShakeAlert uses algorithms to begin calculations of magnitude and intensity of shaking to send out a warning based on instrument data and known velocity models of the localized earth. A countdown of expected shaking also accompanies the message. Depending where the fault rupture begins, ShakeAlert gives from seconds to minutes of warning. Since ShakeAlert does not predict earthquake locations, but only alerts after a rupture starts, the minimum and maximum amount of warning time varies.

In my experience giving tours at the Pacific Northwest Seismic Network (PNSN), the public often asks for guidance when strong shaking occurs. The current suggestion from emergency and risk managers is to drop, cover and hold on (FEMA, 2014; Mahdavifar et al., 2009). This series of actions is drilled in schools where students and others drop down to the ground underneath their desks or tables, cover their heads, and hold on to the leg of the desk or table to protect themselves from falling debris during an earthquake. If more time is expected until strong shaking is felt, a person in a structure may be able to make decisions about sheltering in place versus moving within a safer location in the building or exiting altogether. If the timing to maximum displacement were known for different storied buildings, warnings could be put in place instructing people to exit the building or shelter in place depending on the performance of each building type. To this end, this report examines the range in timing to the first maximum displacement for concrete buildings from 1 to 30 stories using earthquake data from three different field sites: Seattle, Mexico City, and Anchorage. Using three different sites, I can consider if other site-specific factors besides building height and mass, dictate the timing of maximum displacement.

I modeled the timing to maximum building displacement in response to strong ground motion from three specific earthquakes using acceleration data as an input into a single degree of freedom oscillator. Using an open source python code, I modeled building structures as a mass on a spring system using Hooke's Law and Newton's Second Equation of Motion (Figure 4) and the variables of mass, spring constant, and damping ratio. To analyze shear motion the north-south horizontal component of the seismic input was used rather than a vertical component.

Background

Earthquakes and Their Effects on Buildings

Earthquakes deliver energy through seismic waves. When strong enough, these waves can be felt by humans and cause damage or failure to buildings. Seismic waveforms include a P-wave (primary or compressional) followed by an S-wave (secondary or shear wave). It is this secondary wave with a higher amplitude that carries more energy than the P-wave. The higher the amplitude the more displacement the ground experiences. When the amplitude changes suddenly, the ground experiences an acceleration that is detected by strong motion seismic instruments, potentially causing intense shaking and subsequent damage to property and life.

Building and structural failure, often in the form of buckling, relates commonly to poor construction and improper design for seismic loading. Buckling is a form of elastic instability where columns, struts brace and props bend due to sudden, severe structural displacement (Samuel and Weir, 2005).

A rough rule of thumb is that for every additional story, a building's free-vibration period increases by 0.1 second period (Bodin, personal communication, 2018). For a one-story structure, the building moves from its resting place every 0.1 second. A two-story building would vibrate or displace every 0.2 seconds and so on. The taller the building the slower it displaces. During an earthquake, if the ground motion matches the natural resonance period of a building, the displacement of the building will amplify or become larger for some time during and after the earthquake (IRIS, 2019). A common example that most people are familiar with is pushing someone on a swing. Timing the push, or force, of the swing just at the right place in the oscillation, will result in the swing displacing higher, similar to a pendulum. Damping, the slowing or stopping of oscillation, depends on friction and/or the absence of force. Buildings can mimic this oscillation during an earthquake. If structures are poorly built, not up to code or incorrectly designed for seismic loading, buildings can sustain structural damage and possible failure.

Modeling Displacement with a Single Degree of Freedom Oscillator

A common means to assess building displacement is to study the structure's stiffness. Stiffness is defined as the resistance of force against deformation or the load divided by deformation (Baumgart, 2000). Strain, a measure of deformation, is the measure of displacement of an object's dimensions after a force has been applied. To understand dynamic stiffness, a single degree of freedom oscillator can be used to model and quantify building deformation (Priestly and Kowalsky, 2000; Marafi, 2018). The oscillator mimics a mass on a spring to quantify displacement, much like the example of a person being pushed on a swing. With an input forcing function the timing of maximum displacement can be calculated. Knowing when a building's maximum displacement occurs during strong shaking is the outcome that I am focusing on.

Case Study of Seismic Hazards and Tectonic Settings

While the single degree of freedom oscillator can calculate building displacement, it likely takes take into account local ground conditions. The model uses data from one station at a time per earthquake and then iterates per story. To understand the reason for different timing, I have examined the tectonic settings of each location to put the three earthquakes I examined in perspective.

Seattle, Washington and the Puget Sound Basin, USA

The potential seismic hazard in the greater Seattle area is significant as it lies within about 300 kilometers of the Cascadia megathrust fault (see Figure 5) which marks the plate boundary where the Juan de Fuca plate subducts northeasterly beneath the North American plate (Goldfinger et al., 2012). The population of Seattle has increased dramatically since the early 1900s and stands at just over 700,000 (US Census Bureau, 2016). Megathrust or subduction zone earthquakes occur approximately every 300-500 years and can produce up to 9.0+ magnitude earthquakes (Goldfinger et al., 2003). The last known megathrust of Cascadia occurred on January 26, 1700 generating an oceanic tsunami as a result of the magnitude 9.0+ earthquake (Satake et al., 2003; Atwater et al., 1991).

In addition to seismic hazards from a megathrust earthquake, Seattle and the Puget Sound region are at risk for deep intraslab earthquakes which occur on the downgoing plate. Recurrence intervals for deep earthquakes are between 30-50 years and produce up to 7.0+ magnitudes (Wang et al., 2008; Ichinose et al., 2004; Wiest et al., 2007). Three deep earthquakes with greater than magnitude 6.5 have occurred in the last 100 years in the Puget Sound resulting in a total of 17 deaths: 1949 magnitude 7.1, 1965 magnitude 6.5 and 2001 magnitude 6.8 (USGS, 2016). Eight people died each in 1949 and 1965 as a result of the seismic events. Out of these 17 deaths, at least four people died from falling debris and nine people died from heart failure (Lange, 2000). On February 28, 2001, Seattle experienced a magnitude 6.8 deep, intraslab earthquake at 57 kilometers depth and over 51 kilometers from the epicenter. Unreinforced masonry created property damage on soft soils and damage to Sea-Tac International Airport and transportation facilities alone were estimated at $30 million and $86 million, respectively (Ballantyne, 2001).

The third type of earthquake hazard in the Puget Sound region are crustal faults that strike approximately east-west roughly perpendicular to the subduction zone boundary. These faults likely relate to block rotation in the northern Cascadia forearc (Mazzotti et al., 2001; McCaffery et al., 2007; Odum et al., 2016). These include the Seattle Fault Zone, the South Whidbey Island Fault, the Darrington Devils Mountain Fault Zone, the Tacoma Fault Zone, and the Olympia Fault Structure (WA DNR, 2014). These crustal faults are located within the heavily populated Puget Sound Region and can produce magnitude 7.0+ earthquakes. The last known crustal earthquake occurred on the Seattle Fault Zone about 900 AD near Bainbridge Island, Washington, and generated a local tsunami (Pacific Northwest Seismic Network).

Depositional Environment and Geology

The Puget Sound region has experienced repeated periods of extensive glaciation. The most recent glaciation, the Vashon Stade, lasted from 17,400 cal yr BP to 16,400 cal yr BP (Porter and Swanson, 1998). Seattle was covered under about a kilometer of ice that descended from the Cordilleran Ice Sheet. As the glaciers advanced, the ice blocked off the entrance to Puget Sound and its basins creating proglacial lakes (Troost and Booth, 2008). Clay and silt were deposited in impounded proglacial lakes covering sandy deposits and the Olympia beds of the previous interglacial period. This clay layer, the Lawton Clay, consists of hard laminated clay that is an impervious layer (Armstrong et al., 1965). As the glaciers retreated, advanced outwash was deposited in the form of well sorted, medium to fine grained sand with gravel lenses, known as Esperance Sand. (Tubbs, 1974). Overlain on the advanced outwash is unsorted, hard compacted glacial till, known as the Vashon Till (Figure 6 and 7).

While historically Seattle has not experienced a megathrust earthquake, intraslab earthquakes, like Nisqually, have produced seismic amplification and variation within the Seattle basin where different soil types and rock have been identified. This seismic amplification contributes to the damage of buildings (Frankel et al., 2002). During the 2001 Nisqually earthquake, a one Hz amplification shows that Pleistocene stiff soils had a higher peak ground acceleration from 15% to 27% compared to hard rock at 4% (Frankel et al., 2002). Simulations from Nisqually showed that surface waves traveling from the south to the north were a "...result of the velocity contrast across the shallow portion of the basin caused by the presence of the frontal trace of the Seattle fault zone." (Frankel et al., 2009).

Mexico City, Mexico

Seismic hazards are also significant for heavily populated Mexico City as the region lies approximately 360 kilometers from the Middle American Trench (MAT) where the Cocos and Rivera plate subduct northeasterly under the North American plate (Figure 8, Pardo and Suarez, 1995). The population of the city stands at just under 9 million people (US Census Bureau, 2015) and has grown from about 653,000 in 2005. Recurrence intervals shows that megathrust earthquakes occur every 30-60 years along the MAT (Singh and Suarez, 1986). One of the most devastating earthquakes to hit Mexico City was the 1985 Michoacan earthquake that caused several hundred buildings to collapse and resulted in the deaths of nearly 10,000 people (1995, Moreno).

In addition, Mexico City is also at risk for moderate to large earthquakes related to the bending stresses that rupture where the Cocos plate transitions from flat subduction to steeply dipping subduction (Melgar et al., 2018). Recurrence intervals for these types of earthquakes are not known. Three magnitude 6.8-7.1 earthquakes have occurred since 1973 killing at least 660 people (USGS, 2019). The 2017 M_w 7.1 Puebla earthquake was one of these types of earthquakes.

The Mexico City area also experiences seismicity from the nearby Aztlan fault system of the Chichinautzin Range, a volcanic field of Pleistocene-Holocene age. Because earthquakes from this system produce less than roughly a M_w 4 and occur at depths less than 20 km, seismicity in this area is less studied than megathrust or deep earthquakes. However, since 1970 there have

been 70 recorded earthquakes proximal to the range and within the Mexico City basin (Campos-Enriquez et al., 2015).

Depositional Environment and Geology

At the time of the Oligocene, faulting and uplift created the Mexican Trans Volcanic Belt mountains (MTVB). Within the MTVB, resides the Valley of Mexico, a basin of 65 kilometers by 80 kilometers and at an elevation of 2250 meters. During the Pleistocene, volcanic mountains formed with Popocatepetl being the closest and most active stratovolcano near the basin. Within this basin, the forerunner of Mexico City, the Aztec city of Tenochtitlan, was built on an island in the middle of Lake Texcoco (Moreno, 1995). From the time of the Spanish conquest in 1521 to the present, the lake has been drained to accommodate growth. It is this lakebed Mexico City is built upon. The former lakebed deposits consist of lacustrine clay (Tacubaya) interspersed with sand, and volcanic ash and glass.

One of the reasons that the basin in Mexico City experiences seismic amplification is the lacustrine clay deposits, known as Montmorillonite, a type of swelling clay. Atterberg Limits of Mexico City clays show that they have low shear strength and large compressibilities. CU tests of total stress done on Mexico City clays show that the angle of internal friction is between 16 and 22 degrees (Shelley, E.O., 2011). This clay is found at depths between 10 to 80 meters below the ground surface (Moreno, 1985 - Figure 9; Guerrero et al., 2017). Guerrero et al. (2017) site three characteristics that makes this clay deformable, particularly during seismic shaking: saturation of the clay is 200 - 400%, low shear wave velocities of 40 m/s, and high plasticity indexes. In Mexico City during seismic shaking these characteristics translate to a peak spectral acceleration that is 5 to 6 times the peak ground acceleration (Guerrero et al., 2017).

Anchorage, Alaska

The city of Anchorage sits near the northern end of Cook Inlet, bounded to the east by the Chugach Mountains, a result of the Yakutat terrane colliding with Alaska's southern margin since the late or early Miocene (Haeussler et al., 2000,). The Cook Inlet is also the eastern most forearc basin of the Aleutian Subduction Zone (Haeussler et al., 2000, figure 10.). The Alaska-Aleutian subduction zone spans 3800 km and forms the plate boundary between the Pacific and North American plates (Ruppert et al., 2007).

Earthquake hazards to the population of the metropolitan Anchorage (about 400,000 residents) area are significant. Recurrence intervals for megathrust earthquakes are not well known (Ruppert et al., 2017). The most devastating earthquake of historical record was the March 27, 1964 Great Alaskan Earthquake, a megathrust earthquake of M9.2. It occurred near the Prince William Sound approximately 120 km east of Anchorage (UAF, 2018). Felt reports indicated the ground shook for about 4 minutes. In this event 131 people died, mainly from a tsunami that followed the earthquake.

Fourteen magnitude 6+ events have occurred in the last century, including the November 30, 2018 Anchorage earthquake (USGS, 2018). The 2018 Anchorage Earthquake was a magnitude 7.1 similar to the Nisqually Earthquake, in that it was a deep intra slab rupture and was consistent with a normal fault focal mechanism (USGS, 2018). This Anchorage earthquake caused significant landslides and liquefaction that contributed to property damage totally approximately $76 million (USGS, 2018, Demarban, 2018).

Depositional Environment and Geology

The Cook Inlet, a northeast/southeast trending bay, is the easternmost forearc basin in the Alaska-Aleutian Trench. It bounded by uplifted mountains to the east, the Alaska Range and Talkeetna Mountains to the north, and the Aleutian volcanic arc to the northwest (Haeussler et al., 2000). Similar to the Puget Sound region, Cook Inlet has also experienced repeated glaciation during the Quaternary that contribute to glacial and alluvial deposition (Schmoll et al., 1999; Haeussler et al., 2000). It is marked by several northward trending anticlines and synclines (Bouma and Hampton, 1976), lineaments and faults like the Castle Mountain-Lake Clark fault system (Silwal et al., 2018). Since the last glaciation the inlet experiences strong tides that result in smoothing out the bottom of the inlet and forming complex bedding structures like dunes that are up to a kilometer long and ten meters high (Bouma and Hampton, 1976). With high velocity currents fine grained materials, like clay minerals, from the surrounding landscape, get winnowed out and deposited in bays in the inlet, to the Shelikof Strait, the Kodiak shelf and onto the continental slope (Hein et al, 1977).

Stratigraphy of the basin has been dated to the early Eocene (LePain et al., 2017, Figure 11). The Pliocene dated Sterling Formation, along with Quaternary sediments, is up to 3050 m thick consisting of massive sandstones, conglomeratic sandstones and interbedded claystones (Haeussler et al., 2000). The late Miocene Beluga Formation contains interbedded claystone, siltstone, sandstone and lignitic to subbituminous coal of 1100 to 2365 m thick (LePain et al., 2017). It also contains tills and stratified outwash deposits (Haeussler et al., 2000). Beneath the Beluga Formation is the Oligocene to mid-Miocene Tyonek Formation. This formation is reverse faulted against the Beluga Formation and contains massive bedded sandstone and thick coal beds. Underlain is the Oligocene Hemlock formation that consists of sandstone and conglomerates.

The Cook Inlet also experiences seismic amplification due to the geometry of the basin, which consists mainly of sandstone formations atop Middle to Upper Jurassic sediments and Triassic plutonics and bounded on the west by undifferentiated volcanic rock. Crustal thickness of the inlet is 50 km thick (2017, Tape et al.). Seismic noise studies show that the basin is responsible for noise amplification at periods less than 10 s which is within the range of the Anchorage earthquake - about a 1 second dominant period. Three-D seismic imaging of the Cook Inlet basin shows that the inlet has a low velocity anomaly to 24 km (Eberhart-Phillips et al., 2006).

Methods

Single Degree of Freedom Oscillator

To model the timing to maximum building displacement, I adapted an open source python script of a single degree of freedom oscillator (Friedman, 2017). I modified the code to use an accelerogram of a recorded earthquake from a strong motion seismic instrument (see Appendix for code). The code outputs horizontal building displacement based on the number of stories or floors for one station location at a time. The main components of the program are: 1) a forcing function of a second order differential equation, 2) Newton's second law of motion, 3) Hooke's law, and 4) the natural frequency of a mass-spring system.

$$F(0) = mu'' + \gamma u' + ku \quad (1)$$

$$F = ma \quad (2)$$

$$F = -kx \quad (3)$$

$$\omega = \sqrt{k/m} \quad (4)$$

Table 1. Single degree of freedom variables

Variable	Representation	Units
f	force	Newtons
m	mass	kilograms
a, u"	acceleration	meters per second squared
ɣ	damping	kilograms per second
u'	velocity	meters per second
k	spring constant	kilograms per second squared
-k	displacement	meters
ω	natural frequency	rads per second

Input - Seismic Stations

Acceleration data used for the input ground motion was downloaded from the Incorporated Research Institutions for Seismology (IRIS). The IRIS Data Management Center is a repository of data for earthquakes world-wide.

Modern digital seismic instruments record three channels of ground motion, one for each of the three orthogonal directional components. Usually those components are vertical, north-south, and east-west. Since I am interested in building displacement in a shear motion, I chose the

north-south component. Each instrument has a sensitivity or gain (conversion between digital counts and input ground motion amplitude) which had to be accounted for to demean the data to bring those counts to a zero base level. The counts are the outcome of a time dependent function for the duration of the earthquake.

I randomly chose four stations within the regional seismic networks for the three case studies and consistently used the north-south component.

For Mexico City, the code had to be adapted to account for a different file format.

Input Variables

Three variables are needed to satisfy the mass-spring system second order differential equation. I used a total load of 5,410,000 N (Engineering Academy, 2017) per floor and divided by the acceleration of gravity 9.81 m/s^2 to achieve mass in kilograms. Total load includes dead load, the weight of the building, and live load, items that move around the building during the day. For the spring constant of concrete I found a value of 9.8 MN/m (Sakai et al., 2013) and increased until results were not consistent with observation. The upper limit of the value was 11.7 MN/m. To obtain damping, I used a five percent damping ratio (FEMA P695) and multiplied it by critical damping. Critical damping is defined by the other two variables in the following equation:

$$\zeta = c/Cc \tag{5}$$

where ζ is the damping ratio, c is actual damping, and Cc is the critical damping defined by:

$$2 * \sqrt{km} \tag{6}$$

To verify that the output, the building displacement, was reasonable, I compared the results to the actual peak ground acceleration (PGA) and peak ground displacement for the 2001 Nisqually earthquake using a program called Jiggle, an earthquake location program from the Pacific Northwest Seismic Network. In addition for each case study, I also verified PGA for each station channel using the USGS' ShakeMaps or CIRES map for Mexico City.

Timing to Maximum Building Displacement

After the initial test of the model was completed and results verified, I ran the program with three different forcing functions; the 2001 Nisqually, the 2017 Puebla, and the 2018 Anchorage earthquakes. For each earthquake, I ran the simulation for 30 stories for one seismic station at a time. The model provided figures of displacement plotted against time overlain with the acceleration plot. This allowed me to view the displacement in meters of the building against time in seconds (Figures 11, 12, 13).

To determine quantitatively the timing of maximum displacement, I queried when the maximum and minimum displacements occurred from the start of the detection. Since the instrument recorded counts in the north-south direction, the maximum and minimum displacements

represented the maximum displacements in both of those directions. For example in the Nisqually earthquake, for a one story building, there was a maximum displacement of .0599 meters in the north direction at about 14 seconds and another maximum displacement of .0637 meters in the southerly direction at over 14 seconds.

To calculate the absolute time from the start of the rupture, I took the maximum displacement time taken from the recorded start-time, if necessary, and added the time from the rupture time. For example, if an event time was recorded at 18:54:32 and the instrument recorded start time was 18:40, then eight seconds were added to the timing to maximum displacement. I then recorded the displacements with time in a spreadsheet to look for trends (see Appendix).

Results

Results show that the time to maximum building displacement changes with the height of a building as well as station (hypocentral) distance from the rupture, and variation from site to site. To view displacement I plotted the building period from 1.36 to 7.47 seconds (a function of 1 to 30 stories) against the maximum displacement time in seconds per story as a result of the modeling.

Nisqually Earthquake

The Nisqually earthquake shows a range in timing of maximum building displacement between the four stations (HOLY, WISC, MURR, and NOWS) ranging from about 22 to 81 seconds across all building periods (Figure 15). All stations are sampled at 100 Hz.

Station HOLY's maximum displacement times are between 25 and 45 seconds across all periods with the greatest maximum displacement timing of 45 seconds occurring at 2.36 and 2.73 second building periods. A second higher peak maximum displacement timing of 38 seconds occurs at approximately the 4.52 second building period mark and varies slightly downward to just below 32 seconds for the remainder of the building periods. Minimum peak times of 26 and 25 occur at 1.36 and 1.93 building periods and again between at 3.05 and up to the 4.52 second building periods. Timing to greatest maximum displacement would be for buildings between 3 and 4 stories tall and then again between 13 and 17 stories.

Station WISC's maximum displacement times are between 30 and 50 seconds across all periods with the greatest maximum displacement timing of 50 seconds occurring at 2.36 and 2.73 building periods (Figure 15). At the 3.05 building period the timing decreases to 36 seconds. From there the timing to maximum displacement decreases slightly and drops to 32 seconds at the 5.46 second building period. Timing to maximum displacement trends at about 32 seconds and then increases to 33 seconds at the 6.1 second building period and then remains for the 7.47 second building period. Timing to greatest maximum displacement would be for buildings between 3 and 4 stories tall.

Station MURR's maximum displacement times are between 22 and 81 seconds across all periods with the greatest maximum displacement timing of 81 seconds occurring at the 3.86 second building period (Figure 15). MURR's timing to maximum building displacement does not

share the similarities that HOLY and WISC have. Starting at the 1.36 second building period it increases to 58 seconds for two successive periods before dropping back to 25 seconds at the 2.73 second building period. The timing to maximum displacement then increases to 70 seconds at the 3.05 second building period, where HOLY, WISC, and NOWS begin to see a decrease in timing. Maximum displacement time increases again to about 81 seconds at around the 4.00 second building period before leveling off to 48 seconds at the 4.31 building period. It continues to remain at about this timing until the 5.79 second period where timing increases to 61 seconds. Timing increases to a third maximum peak of 75 seconds at the 6.10 second building period. It then again trends at just under this time to the 6.54 second building period before dropping to 46 seconds at the 6.68 period. Timing levels off to 40 seconds at the 7.47 second building period. Timing to greatest maximum displacement would be for building between 8and 9 stories and then again for taller building between 21 and 24 stories tall. A possible explanation for MURR's building response variation compared to the other stations is that it is the closest to the Nisqually hypocenter.

Station NOWS's maximum displacement times are between 32 and 56 seconds across all periods with the greatest maximum displacement timing of 56 seconds occurring at the 4.31 building period (Figure 15). NOWS timing to maximum building displacement shares similarities with MURR across most of the building period range. Like MURR, NOWS starts at about 36 seconds and increases its timing to maximum displacement to 55 seconds at the 2.36 building period. Timing then decreases similarly to MURR at the 2.73 second building period to 33 seconds. Timing remains at about 33 seconds before increasing again to 55 and then to its greatest maximum displacement at 56 seconds at the 4.09 and 4.31 second building periods respectively. Timing then drops to 35 seconds at the 4.52 building period and trends at about this time to the 5.79 second building period. At the 5.95 second building period of 40 seconds, NOWS shows a general increasing trend. At the 6.45 building period of 54 seconds, it levels off through the 7.35 second building period and ends at 42 seconds at the 7.47 second building period. Timing to greatest maximum displacement would be for buildings between 3,6, 9, 10, 23, 24 and 25 stories tall. A possible explanation for its building response site characteristics in comparison to the other three stations is the instrument's sensitivity, which is set at 267825. NOWS is also Whereas HOLY, WISC and MURR are set at 428155.

Examining all four stations for the Nisqually earthquake, in general, the timing to maximum displacement is greatest at just above the 2.0, the 3.0, around the 4.0 second building periods (Figure 18). It also increases again between the 6.0 and 7.0 second building periods for stations MURR and NOWS.

Puebla Earthquake

For the Puebla earthquake, the model shows less variation in amplitude or change in the timing of displacement among the four stations (MI15, JC54, ES57, and BL45) than the Nisqually earthquake (Figure 16). The range in time to maximum displace is from 86 to 103 seconds. All stations are sampling at 100 Hz.

Station MI15 timing to maximum building displacement remains relatively consistent across all building periods with an average timing of 91 seconds (Figure 16). The greatest maximum

timing to building displacement occurs at 93 seconds for the 1.36 second building period or in a short building.

Station JC54 (Figure 16) has similar building response characteristics to station HOLY (during the Nisqually event). Maximum displacement times have increased by approximately 45 seconds and times to maximum displacement increased by a factor of approximately 1.5. It displays more variation than MI15 with peak timings of 94 seconds from the 3.86 to 4.31 second building periods and again at 6.40 to 6.82 seconds. It also has minimum timings of 82 seconds at building periods from 2.36 to 3.61 seconds. Other minimum timing values of 86-87 seconds occur at the 4.52 to 6.10 second building periods, and 88 seconds from the building periods of 6.96 to 7.47 seconds. Timing to maximum displacement for JC54 is greatest at about 9 stories, and again between about 20 to 25 stories tall.

Station ES57 shows an increase is greatest maximum displacement of 101 seconds at the 1.93 building period and then trends downard to a minimum value of about 88 seconds starting from the 3.05 second building period to 4.73 seconds (Figure 16). It then steps up to 99 seconds from the building period 5.95 seconds and then decreases 93 seconds at 6.68 seconds. Timing to maximum displacement increases slightly to 99 seconds for the remainder of the building periods. The highest times to maximum displacement for ES57 show at about 2 stories, and again at about 20 stories tall.

Station BL45 has the most variability of the Puebla earthquake stations with timing to maximum displacement occurring between 86 and 103 seconds (Figure 16). Building response characteristics are similar to Station NOWS for the Nisqually event, although the amplitude changes are decreased about 7 seconds. The greatest time to maximum displacement occurs in taller buildings from about 21-25 stories.

Examining all four stations for the Puebla earthquake, in general, the timing to maximum displacement was greater for taller buildings between the 6.0 and 7.0 second building periods (Figure 19). There was a slight increase around the 4.0 second building period for buildings of about 8 to 12 stories tall. There was another increase around the 2.0 second building period for shorter buildings of about 1 to 2 stories tall.

Anchorage Earthquake

Results for the Anchorage earthquake show some similarity in time to maximum displacement between the 4 stations (Figure 17). The ranges in times were between 22 and 62 seconds. In general the greatest time maximum displacement occur at about the 2 second building period. All stations are sampled at 200 Hz, except for SSN which samples at 50 Hz.

Station K211 shows the greatest time to maximum displacement of 45 and 46 seconds occurs at the 1.93 and 2.36 second building period (Figure 17). Timing decreases to 26 seconds at the 2.73 second building period and then increases to 31 seconds at the 3.34 second building period. Timing remains around 25 and 24 seconds from 3.61 to 5.79 second building periods before increasing again. At the 5.95 second building period it remains at about 30 seconds until the 6.82 second building period. The timing then decreases to 22 seconds for the remainder of

the building periods. The greatest time to maximum displacement of 45 seconds for station K211 occurs for shorter buildings at 2 and 3 stories, and another peak of 30 seconds for taller buildings between 19 to 25 stories.

Station K220 shows the greatest time to maximum displacement of 62 seconds of all four stations (Figure 17). The building response timing range is from 23 to 62 seconds across all building periods. Timing of maximum displacement occurs at the 1.93 second building period. Timing decreases to 50 seconds at the 2.36 second building period and then further to 24 seconds at the 2.73 second building period. It then increases to 32 seconds at the 3.61 second building period and steps down successively to 23 seconds at the final 7.47 second building period. Timing to greatest maximum building displacement would be for shorter buildings of 2 and 3 stories tall.

Station K215 fluctuates to a greatest time to maximum displacement of 42 seconds at the 3.34 second building period (Figure 17). Building response timing range is from 24 to 42 seconds across all building periods. At the 3.61 second building period timing is at 24 seconds and fluctuates within about a 2 second window until the final 7.47 second building period. Timing to the greatest maximum building displacement would be for a six story tall building.

Station SSN has a somewhat muted response for timing to maximum displacement compared to the other three stations but has similar characteristics to K211 and K220 (Figure 17). The timing to maximum displacement ranges from 24 to 33 seconds across all building periods. Timing to the greatest maximum displacement of 33 seconds occurs at the 1.93 second building period. Timing begins at 29 seconds, increases to 33 seconds and then decreases to 24 seconds at the 2.73 second building period. It then increases to 32 seconds where it remains up to the 5.46 second building period. It then decreases to 28 seconds for the remainder of the building period range. The greatest timing to maximum displacement for SSN is shorter buildings from 2 to 3 stories at 33 and 32 seconds and then again at 32 seconds for 14 to 16 storied buildings. Possible explanations for the building response at SSN is station gain, 427894 and sample rate of 0.02 seconds. K211, K220, and K215 all had gains of 213947 with sample rates of 0.005 seconds.

Examining all four stations for the Anchorage earthquake, in general, the timing to maximum displacement was greater for shorter buildings of 2 to 3 stories tall around the 2.0 second building period (Figure 20). Minimal time to maximum displacement of about between 24 and 26 seconds occurred for all stations at the 2.73 second building period for about a 4 story building. Except for station K215, which shows an increase at the 3.34 second period, the stations show a decreasing time to maximum displacement as building height increases. This may be a function of the distance to the hypocenter.

Discussion

While each earthquake was tectonically similar with nearly similar magnitudes, the building responses were different based on the seismic station at its location (Figure 21). The model does not require soil or bedrock conditions or velocity models. The output was only based on the input of the forcing function (the acceleration) and the variables of mass, spring constant and the damping ratio. However, instrument responses more than likely reflect surface

conditions. Other factors that could influence building responses are the sampling rate and the sensitivity or gain for instrument data downloaded from IRIS. Station data from CIRES is already converted to units of acceleration.

One reason for the differences in timing to maximum displacement, could be the distance of the rupture to the station location. There is a strong correspondence between the time when energy within a frequency band arrives that is at the free-period of a structure and the time when maximum displacement (and therefore damage) is attained. For Nisqually earthquake, the average hypocentral distance was approximately 74 kilometers away while the Anchorage earthquake was an average of 56 kilometers from the hypocenter. The average distance to the Puebla earthquake hypocenter for the Mexico City instruments was 122 kilometers. It is more than likely the reason that building responses were less variable for the Puebla earthquake is due to the greater distance to the rupture compared to the Nisqually and Anchorage earthquakes. In general the timing to maximum displacement was at about 82 seconds for all building periods. The overall timing to maximum building displacement increased on average between 50 to 60 seconds compared to the other two earthquakes. The timing to maximum displacement was greatest for longer building periods suggesting that surface waves dominated the ground motion. The results suggest that more distant, but stronger earthquakes, would likely allow for longer warning times since slow-moving long-period surface waves might dominate ground motions. For the Anchorage earthquake energy was dissipated closer in the area and higher frequency waves dominated the building response results for the four stations.

Duration of the rupture and when the strongest shaking occurred, could affect at what building period the timing to maximum displacement occurs. A look at the seismogram at HOLY shows that strong shaking lasted for about 20 seconds. Maximum displacement occurs after the 2.0 period, at about 3.0, 4.0 and between 6.0 and 7.0 second building periods. For Anchorage strong shaking was more intense and earlier than Nisqually, lasted about 12 seconds and maximum displacement was at the 2.0 second building period. Puebla had strong shaking for about 25 to 30 seconds and with greater peak accelerations than Anchorage. However taller buildings would experience the greatest maximum displacement.

It is possible that in addition to instrument sensitivity, duration, and distance from rupture the surficial deposits may contribute to these differences. In the case of the Nisqually earthquake, station HOLY rests on Vashon recessional outwash, WISC on alluvial fan deposits, MURR on recessional outwash and Steilacoom gravel, and NOWS on Vashon till (Troost and Booth, 2008; Washington Geologic Portal, 2019; Norman, 2015). Since they all rest on quaternary glacial deposits this may be the least likely explanation for their differences. However MURR and NOWS show similar patterns and are on deposits that contain sand and gravel. Another possible contribution to these variations could be the directivity of the energy from the rupture as it enters the basin to these sites and the path the energy takes through the region's heterogeneous layers.

For the Puebla earthquake the four stations all resided on quaternary alluvium deposits, mainly of clay, that are underlain by a relatively more uniform stratified layers of increasingly competent soil layers and basement rock than the Puget Sound Basin. It is possible that the long period surface waves from the farther afield rupture entering the more bowl shaped, unformed layer of Mexico Valley could explain the more uniform building response results.

For the Anchorage earthquake the four stations resided on quaternary glacial deposits, estuary deposits, and volcanic rock. Stations K211 rests on glacioestuarine deposits, K220 on Holocene estuarine deposits, K215 on major moraine and kame deposits, and SSN on quartz diorite (Wilson et al., 2012).

While not part of this analysis, the question of drift ratio was asked by the author when examining displacement. How much displacement could occur to a building before a structure could fail? Drift ratio is the change in displacement per story divided by the height of the story (FEMA 454, 2006). The IBC requires that drift displacement be limited to between 0.01 and 0.02 times the building height (FEMA 454, 2006). According to the model, for the three events only one and two story buildings came within significant range of the limits but did not exceed the limits (Figures 24, 25, 26, 27, and 28). This contradicts damage to buildings in the Puebla events where buildings of up to 8 stories collapsed (Sackman field observations, 2019 - see Appendix). The discrepancy could be due to failure to follow building codes or due to the amplification of the Mexico City basin that the model does not take into account.

Lastly, a couple of final points should be addressed briefly: 1) The placement of the seismic instruments are typically at ground level. So the single degree of freedom oscillator model is only calibrated to the center of mass of the building; 2) additional displacements could be examined in the east-west directional component to obtain a more complete analysis of shear motion; 3) analysis of potential and kinetic energy could also be completed as the model is capable of performing those calculations; 4) other types of earthquakes like strike-slip or compression fault motions have not been examined with this model; 5) it should be noted that no analysis or metric was examined to look at how long it would take for people to evacuate or exit a building structure during strong shaking.

Conclusion

In conclusion, three normal fault, deep earthquakes of similar magnitude were modeled using a single degree of freedom oscillator program in Python code to examine the timing of maximum building displacement. With the advent of earthquake early warning (EEW), it is now possible to know when strong shaking from an earthquake occurs to at-risk populations. If the timing of maximum displacement were known, then other life-saving actions could be taken to evacuate an at-risk or fragile building. Findings indicate that the single degree of freedom model shows that in general, the closer the rupture is to a seismic station, shorter buildings have the greatest time to maximum displacement. For the Nisqually event the first maximum displacement time is the greatest at between 45 and 55 seconds (and in one case over 75 seconds) for a 2.0, 3.0 and 4.0 building period. There is also a 50 to 75 second maximum time between the 6.0 and 7.0 building period. The Puebla earthquake shows overall increased time compared to the Nisqually and Anchorage earthquakes. In one location the time to maximum displacement is close to 100 seconds at a building period of about 2.0 seconds. Another peak time to maximum displacement occurs at over 100 seconds between the 6.0 and 7.0 building periods. The Anchorage event shows first maximum displacement time from 30 to over 52 seconds for a 2.0 building period and again between 30 to 42 second maximum time between the 3.0 and 4.0 second building period.

For the Nisqually and Anchorage earthquakes the public would have the maximum amount of warning time to take life saving action in some lower storied buildings before the first maximum displacement occurs. At the MURR station location for Nisqually for about a 20 story building, the public would have just under a minute. At the K215 station for the Anchorage earthquake, the public would also have 42 seconds to take action between a 5 to 9 story tall building.

In the case of the Puebla earthquake, the minimum amount of time for all periods, from 1.36 to 7.22 second periods is about 82 seconds for all stations examined. For lowered storied buildings the public may have time to shelter in place, move within the building to a safer location or exit the building. The greatest time to maximum displacement at station BL45 is at about 103 seconds at a higher storied building. Depending on what story an individual is on, this may not be enough time to exit the building. In this instance it may be wise to shelter in place or find a safer place within the building.

All three areas have slightly different depositional environments and surface geology that give rise to basin effects. Seismic amplifications and soil conditions are not input into the model, but are probably recorded in the displacement output. An examination of different stations for each earthquake would give a more comprehensive analysis into the timing of building displacement. It should be noted that stations MURR and NOWS (Puget Sound region) and K215 (Cook Inlet) have similar characteristics. These three stations show similar patterns in building response and are located on recessional outwash and Steilacoom gravel, Vashon till, and major moraine and kame deposits, respectively, which consist of sand, gravel, and till. Gravel is present in all three of these deposits and may play a role in this pattern.

In addition, each location, while all three in subduction zones, has different recurrence intervals and different aftershock sequences. If there are several aftershocks immediately after the mainshock, like in the Puebla and Anchorage earthquakes, this could increase the risk of building displacement and subsequent building damage that would not be detected in the model.

Modeling building displacement using a single degree of freedom oscillator is a solid first step in examining the timing of maximum displacement during intense seismic shaking. Quantifying when ground movement is detected and when maximum displacement occurs can give a good approximation of the amount of time someone has to take action when in a structure. Partnering this study with earthquake early warning would also be a good first start to potentially save lives.

References

1. Armstrong, J.E., Crandell, D.R., Easterbrook, D. J., and Noble, J.B., 1965, “Late Pleistocene stratigraphy and chronology in southwestern British Columbia and northwestern Washington”, Geological Society of America Bulletin, v. 76, p. 321 - 330, doi: 10.130/0016-7606(1965)76 [321 :LPSACI]2.0.CO:2.
2. Astiz et al., 1987, “Source Characteristics of Earthquakes in the Michoacan Seismic Gap in Mexico”, Bulletin of the Seismological Society of America, Vol. 77, No. 4, pp. 1326-1346, August 1987.
3. AESI, 2017 (personal communication, Troost, 2018).
4. Ballantyne, D., 2001, “The Nisqually Earthquake of 28 February, 2001, Preliminary Reconnaissance Report”, Nisqually Earthquake Clearinghouse Group, University of Washington, Seattle, WA.
5. Baumgart, F., 2000, “Stiffness - an unknown world of mechanical science?”, Injury, Elsevier
6. Bojórquez, J., et al., 2017, “Reliability-based optimal load factors for seismic design of buildings”,Engineering Structures, 151, 527–539.
7. Campos-Enriquez, J.O., Lermeo-Samaniego, J.F., Antayhua-Vera, Y.T., Chavacán, M., Ramón-Márquez, V.-M., 2015, “The Aztlán Fault System: control on the emplacement of the Chichinautzin Range volcanism, southern Mexico Basin, Mexico. Seismic and gravity characterization”, Boletin de la Sociedad Geologica Mexicana, Volumen 67, Num. 2, 2015, p. 315-335.
8. CIRES, http://www.cires.org.mx/racm_mapa/index.php (accessed March, 2019).
9. Czajkowski, J.L. and Bowman, J.D., 2014-05, “Faults and Earthquakes in Washington State”, Washington Division of Geology and Earth Resources Open File Report.
10. Mayoral, J.M., et al., 2017, “Regional subsidence effects on seismic soil-structure interaction in soft clay”, Soil Dynamics and Earthquake Engineering, 103, 123–140.
11. FEMA 454, 2006, “Risk Management Series, Designing for Earthquakes, A Manual for Architects.
12. FEMA, 529, 2014, “Drop, Cover, and Hold On Poster (FEMA 529)”, https://www.fema.gov/media-library/assets/documents/3266
13. FEMA P695, 2009, “Quantification of Building Seismic Performance Factors:, Applied Technology Council
14. Frankel et al., 2002, “Nonlinear and Linear Site Response and Basin Effects in Seattle for the M 6.8 Nisqually, Washington, Earthquake”, Bulletin of the Seismological Society of America, Vol. 92, No. 6, pp. 2090–2109, August 2002.
15. Frankel et al., 2009, “Sedimentary Basin Effects in Seattle, Washington: Ground Motion Observations and 3D Simulations”, Bulletin of the Seismological Society of America, Vol. 99, No. 3, pp. 1579–1611, June 2009, doi: 10.1785/0120080203.
16. Friedman, A., 2017, https://www.youtube.com/watch?v=-WhS5iuvGr0&t=1361s (aka Freeball, accessed May, 2018).

17. Graham, S., et al., 2016, “Slow Slip History for the MEXICO Subduction Zone: 2005 Through 2011”, Pure Applied Geophys. 173 (2016) 3445-3465, DOI 10.1007/s00024-015-1211-x.
18. Grillo, I., 2017, Time Magazine, http://time.com/4954580/mexico-city-earthquake-collapse-building-codes-block/ (accessed March, 2018).
19. Guerrero, H., et al., 2017, “Response to seismic sequences of short-period structures equipped with Buckling-Restrained Braces located on the lakebed zone of Mexico City”, Journal of Constructional Steel Research, 137, 37–51.
20. Haeussler, P.J., Bruhn, R. L., Pratt, T. L., 2000, “Potential seismic hazards and tectonics of the upper Cook Inlet basin, Alaska, based on analysis of Pliocene and younger deformation”, GSA Bulletin, September 2000, v. 112112; no. 9; p. 1414–1429; 9 figures; 3 tables.
21. Hein, J.R., Bouma, A.H., Hampton, M.A., 1977, U.S. Geological Survey, Open File Report 77-581, Menlo Park, California, July 1977.
22. Ichinose, G.A., Thio, H.K., Somerville, P.G., 2004, “Rupture process and near-source shaking of the 1965 Seattle-Tacoma and 2001 Nisqually, intraslab earthquakes”, Geophysical Research Letters, VOL. 31, L10604, doi:10.1029/2004GL019668.
23. IRIS, https://www.iris.edu/hq/inclass/animation/building_resonance_the_resonant_frequency_of_different_seismic_waves (accessed April, 2019).
24. Johson, S.Y., Potter, C.J., Armentrout, J.M., 1994, “Origin of the evolution of the Seattle Fault and Basin, Washington”, Geology, Vol.22(1), pp.71-74, https://doi-org.offcampus.lib.washington.edu/10.1130/0091-7613(1994)022<0071:OAEOTS>2.3.CO;2.
25. Kenny, Charles, 2009, “Why Do People Die in Earthquakes? The Costs, Benefits and Institutions of Disaster Risk Reduction in Developing Countries”, The World Bank, Sustainable Development Network, Finance Economics & Urban Department, Policy Research Working Paper 4823.
26. Lange, G. , “Earthquake rattles Western Washington on April 29, 1965, History Link.org, https://www.historylink.org/File/1986 (accessed, December, 2018).
27. Lange, G., “Earthquake hits Puget Sound area on April 13, 1949”, History Link.org, https://www.historylink.org/File/2063 (accessed, December, 2018).
28. Leonard, L.J., Currie, C.A., Mazzotti, S., and Hyndman, R.D., “Rupture area and displacement of past Cascadia great earthquakes from coastal coseismic subsidence”, GSA Bulletin; November/December 2010; v. 122; no. 11/12; p. 2079–2096; doi: 10.1130/B30108.1.
29. LePain, D.L., Helmold, K.P., Gillis, R.J., Reger, R.D., Swenson, R.F., 2017, “Field Trip Guidebook Sedimentology, Reservoir Quality, and Tectonic Setting of Late Miocene-Early Pliocene Gas-Bearing Formation, Upper Cook Inlet, Alaska”, Alaska Division of Geological & Geophysical Surveys, Miscellaneous Publication 161.
30. Li, Shuang ; Yu, Xiaohui ; Zhang, Yanjuan ; Zhai, Changhai, 2018, “A numerical simulation strategy on occupant evacuation behaviors and casualty prediction in

a building during earthquakes", Physica A: Statistical Mechanics and its Applications, 15 January 2018, Vol.490, pp.1238-1250.
31. Mahdavifar, M.R. , Izadkhah, Y.O., and Heshmati, V., 2009, "Appropriate and Correct Reactions during Earthquakes: 'Drop, Cover and Hold on' or 'Triangle of Life'", JSEE, Spring 2009, Vol. 11, No. 1.
32. Marafi, N.A., 2018, "Impacts of an M9 Cascadia Subduction Zone Earthquake on Structures Located in Deep Sedimentary Basins", Dissertation, University of Washington
33. Manzotti, S., Draggert H., Hyndman, R.D., Miller, M.M., and Henton, J.A., 2002, "GPS deformation in a region of high crustal seismicity: N. Cascadia Forearc", Earth and Planetary Science Letters, v. 198, p. 41-48, doi: 10 .1016 /S0012 -821X (02)00520 -4 .
34. McCaffrey, R., Qamar, A.I., King, R.W., Wells, R., Khazaradze, G., Williams, C.A., Stevens, C.W., Vollick, J.J., and Zwick, P.C., 2007, "Fault locking, block rotation and crustal deformation in the Pacific Northwest", Geophysical Journal International, v. 169, p. 1315–1340, doi: 10.1111 j.1365 -246X .2007 .03371 .x.
35. McCaffrey, R., King, R., Payne, S.J., and Lancaster, M., 2013, "Active tectonics of northwestern U.S. inferred from GPS-derived surface velocities", Journal of Geophysical Research, v. 118, p. 1–5, doi: 10 .1029 /2012JB009473.
36. Melgar, D., Pérez-Campos, X., Ramirez-Guzman, L., Spica, Z., Espíndola, V. H., Hammond, W. C., & Cabral-Cano, E. (2018). Bend faulting at the edge of a flat slab: The 2017 Mw7.1 Puebla-Morelos, Mexico Earthquake.Geophysical Research Letters, 45, 2633–2641. https://doi.org/10.1002/2017GL076895.
37. Mexican Seismic Design Code (2004), Complimentary Technical Norms for Seismic Design (in Spanish, Normas Tecnicas Complementarias Para Disenso Por Sismo).
38. NOAA, Geologic Hazards Photos Volume 2 Earthquake Events, ftp://ftp.ngdc.noaa.gov/hazards/cdroms/geohazards_v2/document/647003.htm, (accessed March, 2018).
39. The News Tribune, https://www-1.thenewstribune.com/news/local/article228847839.html (accessed December, 2018).
40. Pacific Northwest Seismic Network, https://pnsn.org/outreach/earthquakesources/csz, accessed, March, 2018).
41. Pardo, M., Suarez, G., 1996, Shape of the subducted Rivera and Cocos plates in southern Mexico: Seismic and tectonic implications, Journal of Geophysical Research, Vol. 100, No. B7, pages 12,357 - 12,373, July 10, 1995.
42. Perez-Campos et al., 2008, Horizontal subduction and truncation of the Cocos Plate beneath central Mexico: Geophysical Research Letters, v. 35, L18303, https:// doi .org /10 .1029 /2008GL035127.
43. Porter, S.C., and Swanson, T.W., 1998 "Radiocarbon age constraints on rates of advance and retreat of the Puget Lobe of the Cordilleran Ice Sheet during the last glaciation", Quaternary Research, v. 50, p. 205 - 213, doi: 10.1006/qres.1998.2004
44. Priestly, M.J.M, and Kowalsky, M.J., 2000, "Direct Displacement-Based Seismic Design of Concrete Buildings", Bulletin of the New Zealand Society for Earthquake Engineering, Vol. 33, No. 4, December 2000

45. Ruiz-García, J. and Guerrero, H, 2017, “Estimation of residual displacement ratios for simple structures built on soft-soil sites”, Soil Dynamics and Earthquake Engineering 100, 555–558.
46. Ruppert, N., Lees, J.M., and Kozyreva, N.P, 2007, “Volcanism and Subduction: The Kamchatka Region”, Geophysical Monograph Series 172 Copyright 2007 by the American Geophysical Union. IO.1029/172GMI2 Volcanism and Subduction : The Kamchatka Region, edited by John Eichelberger, et al., American Geophysical Union, 2007. ProQuest Ebook Central, http://ebookcentral.proquest.com/lib/washington/detail.action?docID=1184593.
47. Sakai, T., Kubo, G., Kubo, H, 2013, “Theoretical considerations on estimation of compressive strength of concrete by means of hammer blowing”, Sustainable Construction Materials and Technologies, 2013, Vol.2013-
48. Savage, W.Z., Morrissey, M.M., Baum, R.L., 2000, Geotechnical Properties for Landslide-Prone Seattle --Area Glacial Deposits, U.S. Geological Survey Open File Report 00-228.
49. Schmoll, H.R., Yehle, L.A., Updike, R.G., 1999, “Summary of Quaternary geology of the Municipality of Anchorage, Alaska”, Quaternary International, 60 (1999) 3-36.
50. Shearer, P, 2009, “Introduction to Seismology, 2nd Edition”, New York, Cambridge University Press, 245-264.
51. Schuster, J.E., Cabibbo, A.A., Schilter, J.H., Hubert, I.J., 2015, “Geologic Map of the Tacoma 1:100,000-Scale Quadrangle, Washington”.
52. Silwal, V., Tape, C., Lomax, A., 2018, “Crustal earthquakes in the Cook Inlet and Susitna region of southern Alaska”, Tectonophysics, 745 (2018) 245-263.
53. Shelley, E.O., 2011, “Some Geotechnical Properties to Characterize Mexico City Clay”, Instituto de Ingeniería UNAM, México, 2011 Pan-Am CGS Geotechnical Conference.
54. Singh, S.K. and Suárez, G., 1986, “Review of the seismicity of Mexico with emphasis on the September 1985, Michoacan earthquakes”, Instituto de Geofísica, UNAM.
55. Tape, C, Christensen, D., Moore-Driskell, M.M., Sweet, J., Smith, K., “Southern Alaska Lithosphere and Mantle Network (SALMON): A Seismic Experiment Covering the Active Arc by Road, Boat, Plane, and Helicopter”, Seismological Research Letters, Volume 88, Number 4, July/August 2017, p. 1185 - 1202, doi 0.1785/0220160229
56. Telesca L., et al., 2018, “Time-reversibility in seismic sequences: Application to the seismicity of Mexican subduction zone”, Physica A, 492, 1373-1381.
57. Troost, K.G., Booth, D.B., 2008, “Geology of Seattle and the Seattle area, Washington”, The Geological Society of America Reviews in Engineering Geology, v. XX, p. 1-35, doi: 10.1130/20084020(01).
58. Tubbs, D.W., 1974, “Landslides in Seattle: Washington Division of Geology and Earth Resources Information Circular” 52,15 p.
59. United Nations Office for Disaster Risk Reduction, “Why Do People Die in earthquakes? Buildings are the main killers”.,https://www.unisdr.org/archive/8813 (accessed, April, 2019)

60. US Census Bureau, 2016, https://www.census.gov/search-results.html?q=Seattle+city%2C+WA&page=1&stateGeo=none&searchtype=web&cssp=Typeahead&%3Acq_csrf_token=undefined (last accessed, March, 2018).
61. US Census Bureau, National Institute of Statistic and Geography, 2010, https://www.google.com/search?q=mexico+city+population&rlz=1C5CHFA_enUS723US723&oq=mexico+city+population&aqs=chrome..69i57.4152j0j7&sourceid=chrome&ie=UTF-8 (last accessed, March, 2018).
62. USGS, https://earthquake.usgs.gov/data/rupture/directivity.php, (access March, 2018).
63. USGS, https://earthquake.usgs.gov/learn/today/index.php?month=10&day=24&submit=View+Date (accessed, May, 2019).
64. USGS, https://earthquake.usgs.gov/earthquakes/eventpage/usp0009f7v/impact (accessed, May, 2019).
65. USGS, https://earthquake.usgs.gov/earthquakes/browse/stats.php, (accessed April, 2019).
66. USGS, https://earthquake.usgs.gov/earthquakes/eventpage/us1000hyfh/executive (accessed December, 2018).
67. USGS, https://archive.usgs.gov/archive/sites/www.usgs.gov/newsroom/article.asp-ID=482.html
68. USGS, https://earthquake.usgs.gov/earthquakes/eventpage/ak20419010/ground-failure/summary (accessed December, 2018).
69. USGS, https://earthquake.usgs.gov/research/earlywarning/background.php, (accessed April, 2019).
70. USGS, "M 6.8 - Seattle-Tacoma urban area, Washington", https://earthquake.usgs.gov/earthquakes/eventpage/ushis1657/executive
71. UAF (University of Alaska Fairbanks), https://earthquake.alaska.edu/earthquakes/notable/1964-m92-great-alaskan-earthquake (accessed, December 2018).
72. Washington Geologic Portal, https://geologyportal.dnr.wa.gov/ (accessed, May, 2019).
73. https://www.historylink.org/File/2063
74. Wilson, F.H., Hults, C.P., Schmoll, H.R., Haeussler, P.J., Schmidt, J.M., Yehle, L. A., Labay, K.A., 2012, "Geologic Map of the Cook Inlet Region, Alaska, Including parts of the Talkeetna, Talkeetna Mountains, Tyonek, Anchorage, Lake Clark, Kenai, Seward, Iliamna, Seldovia, Mount Katmai, and Afognak 1:250,000-scale Quadrangles", USGS.

Figures

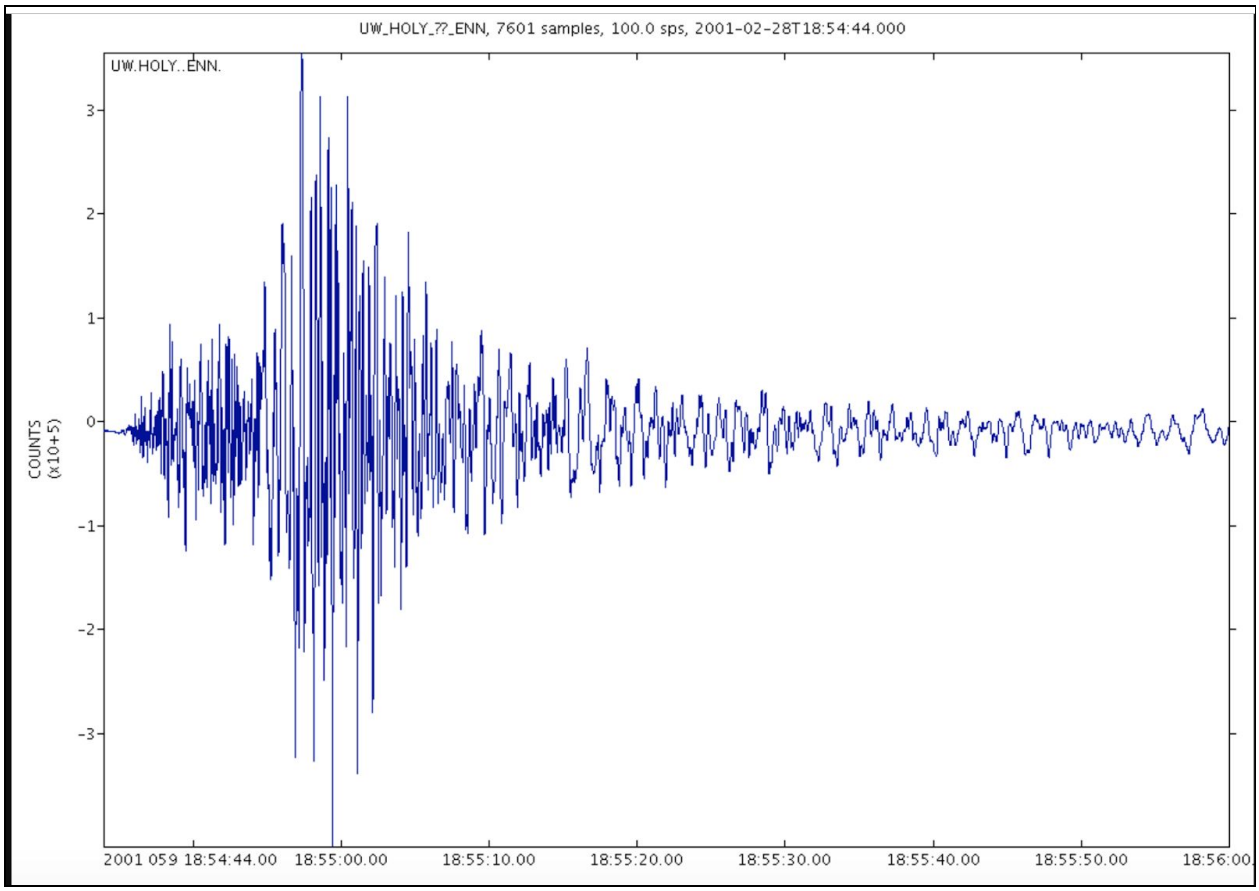

Figure 1. Seismogram at station HOLY during the 2001 Nisqually Earthquake.

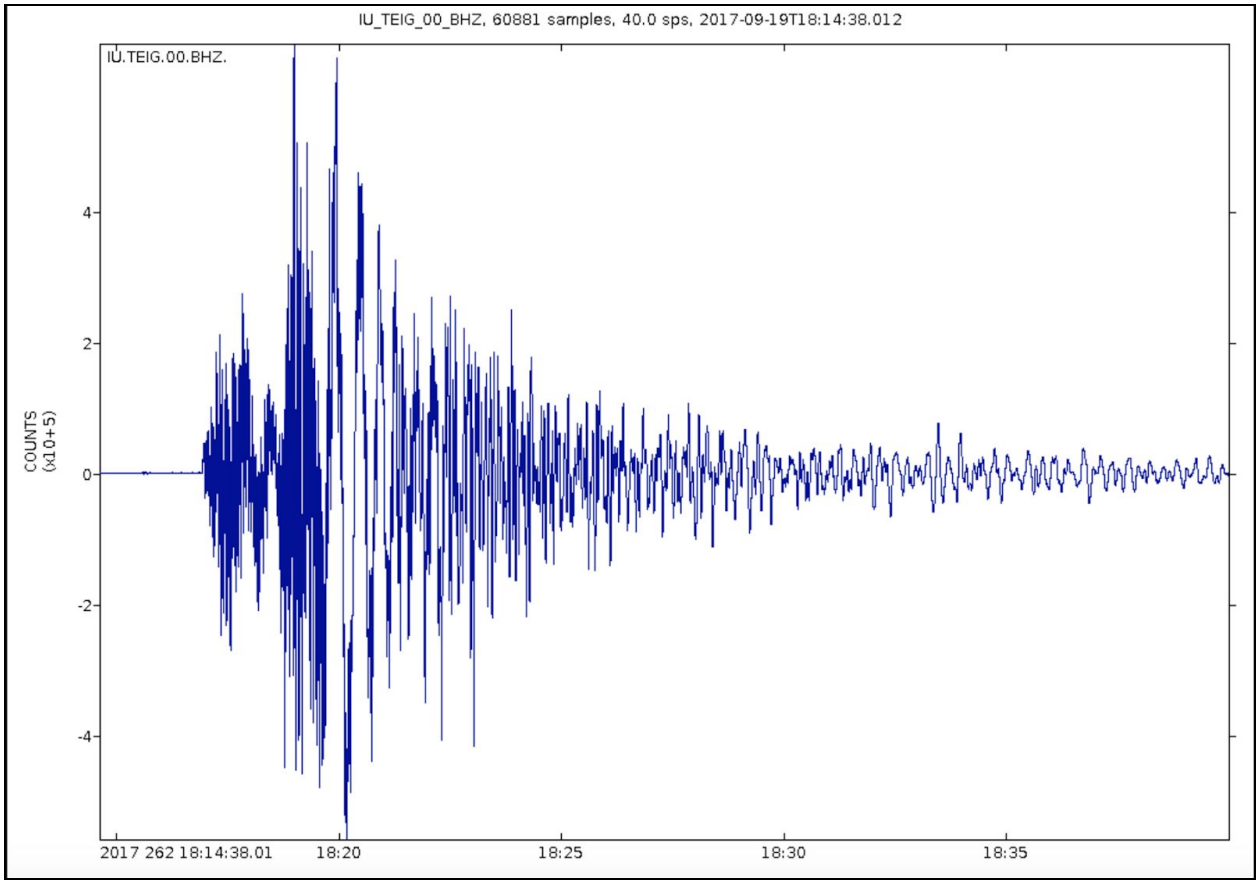

Figure 2. Seismogram at station TEIG during the 2017 Puebla Earthquake.

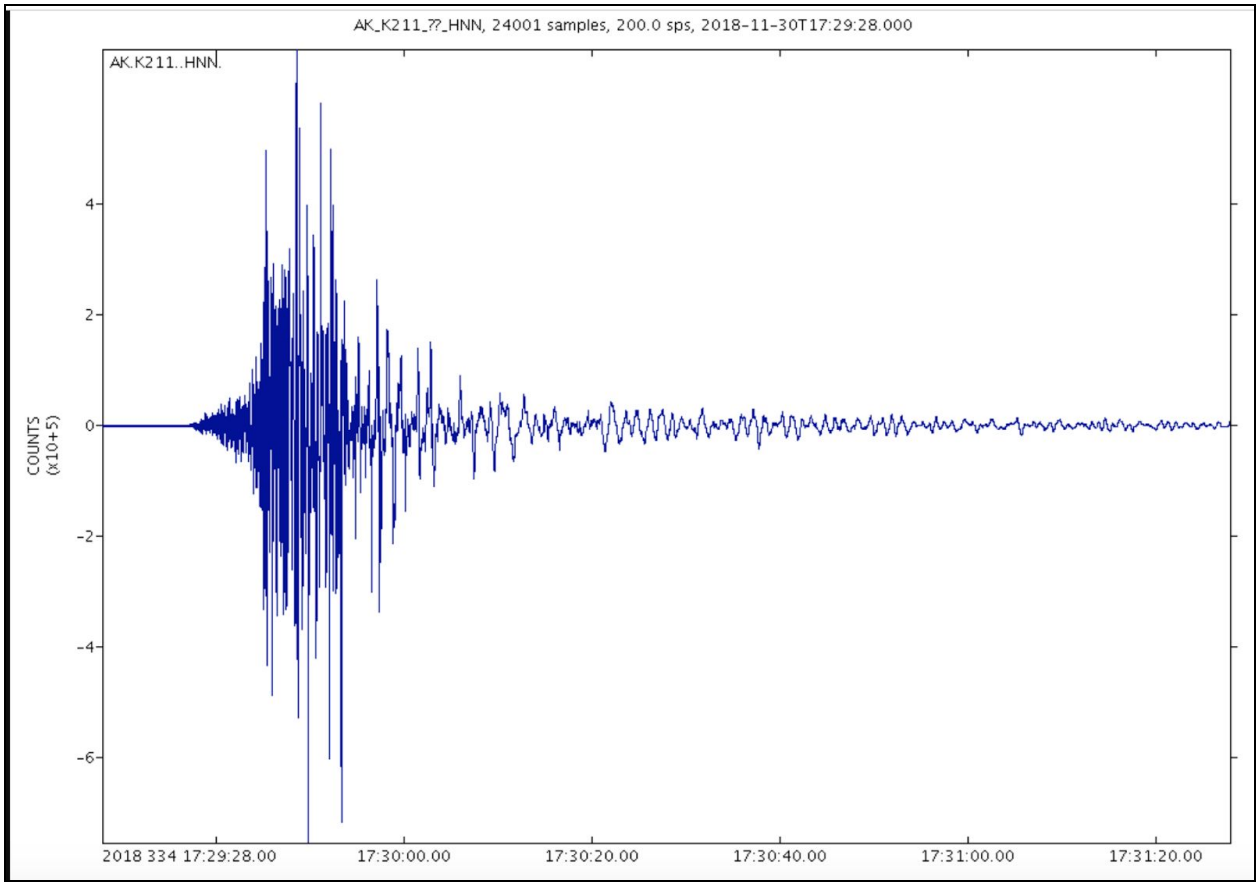

Figure 3. Seismogram at station K211 during the 2018 Anchorage Earthquake.

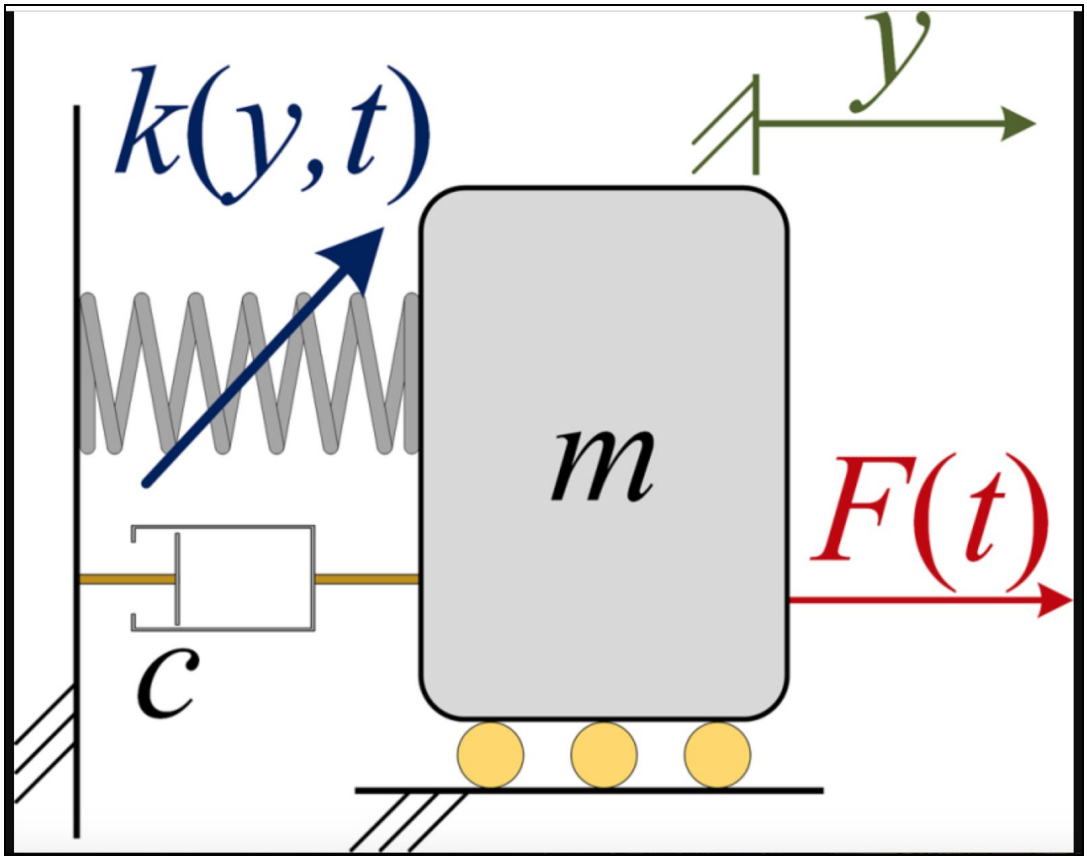

Figure 4. Mass-spring system with displacement - Dolev and Bucher, 2016.

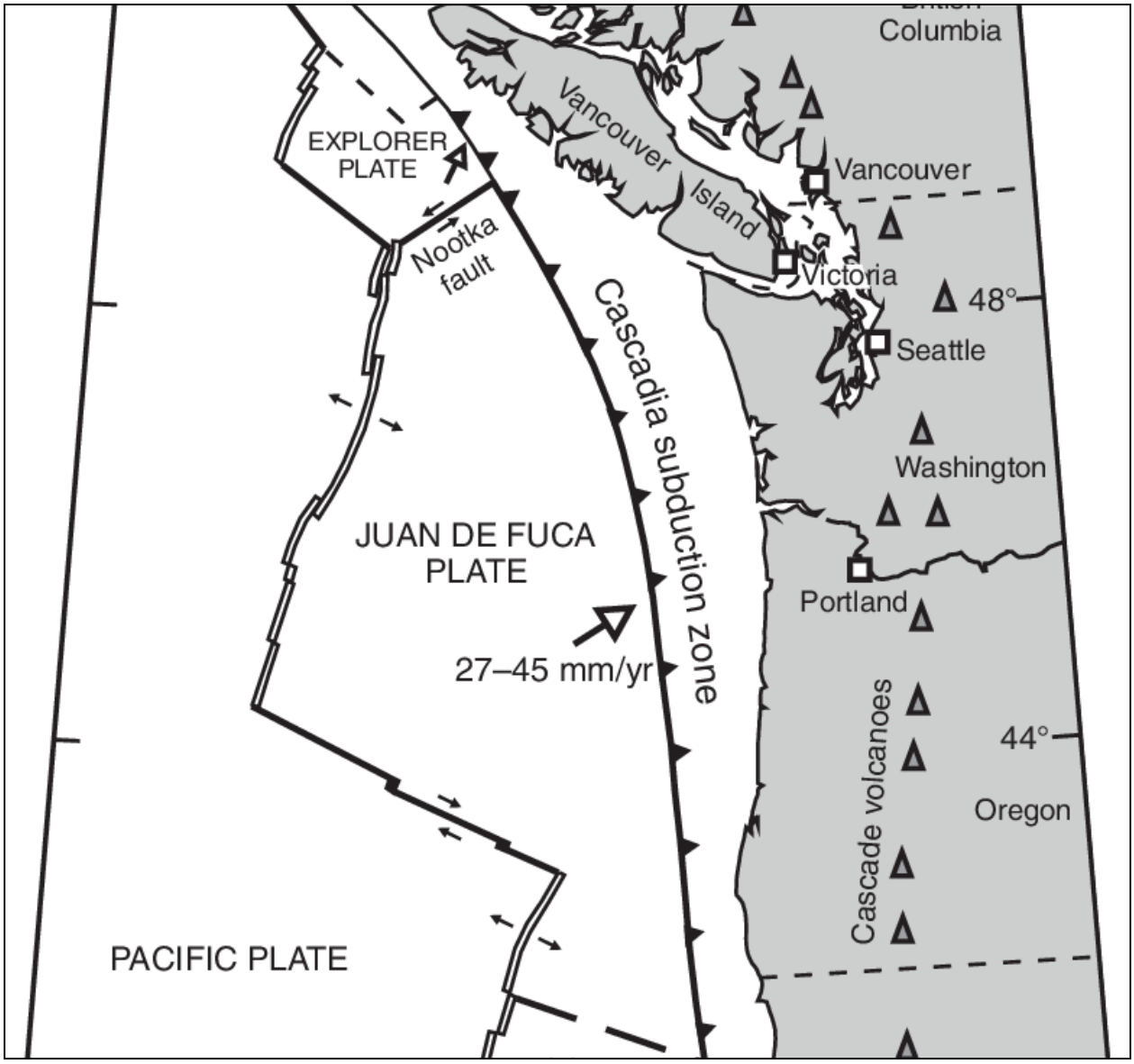

Figure 5. Sources of earthquakes in the Pacific Northwest from the subducting Juan de Fuca Plate - Leonard et al., 2010.

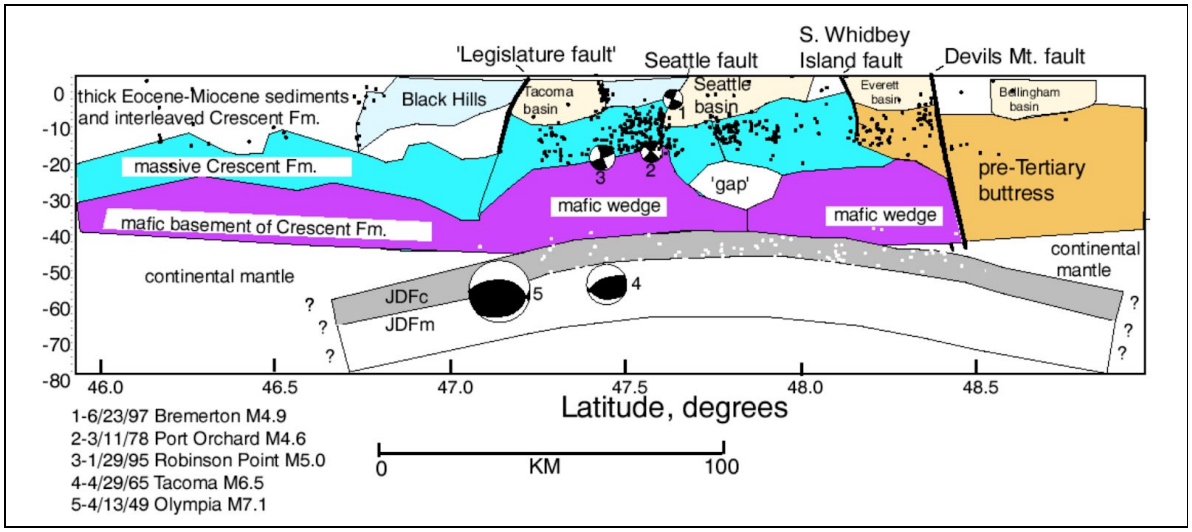

Figure 6. Cross section of faults in the Puget Sound Region - USGS, 1999.

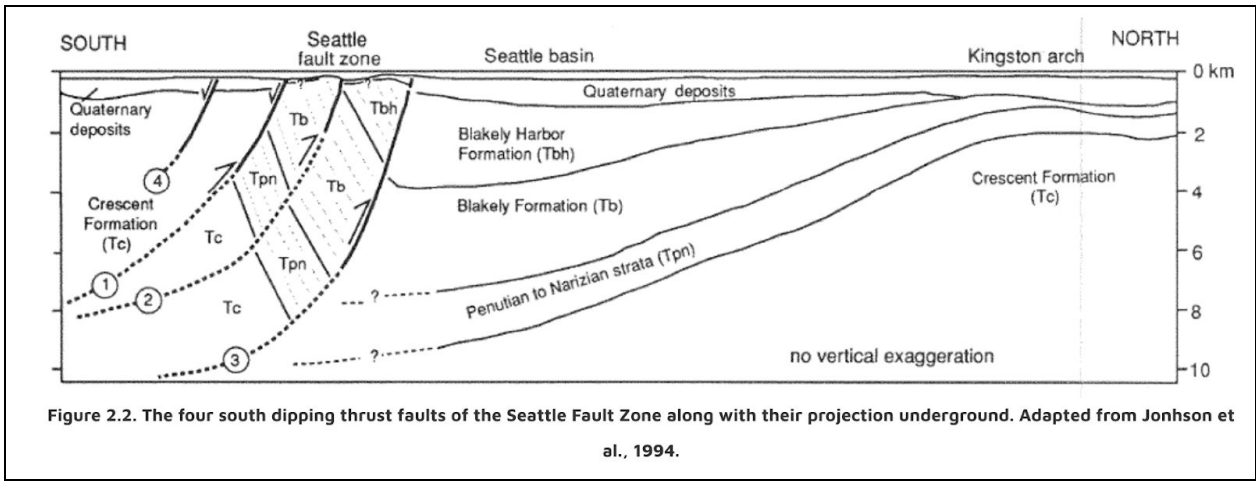

Figure 7. Seattle basin cross section - Johnson et al., 1994

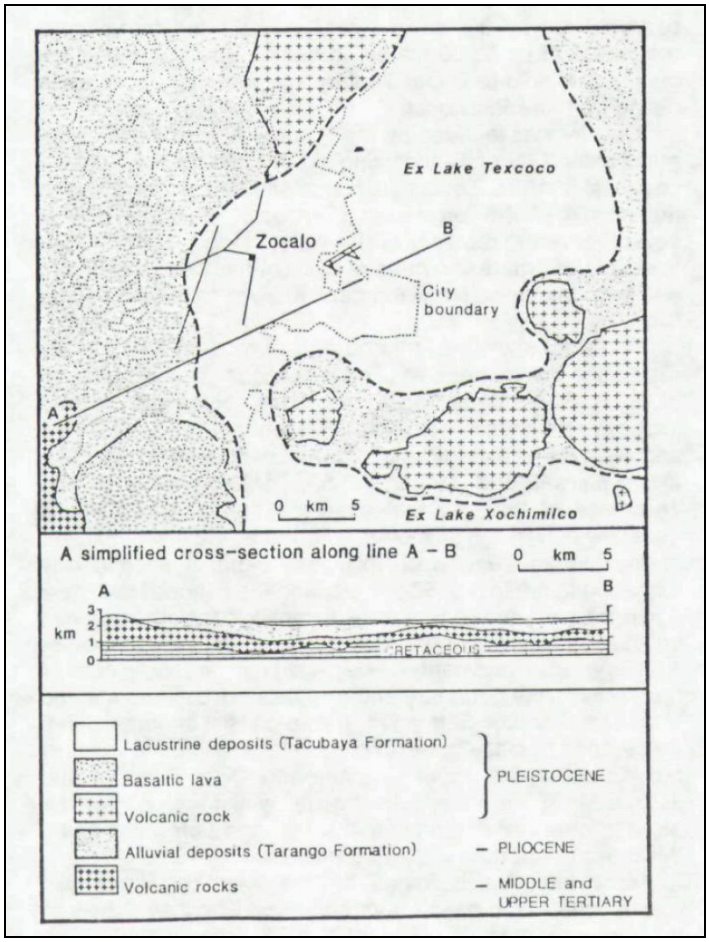

Figure 8. Mexico City Basin - Moreno, J. M. (1995).

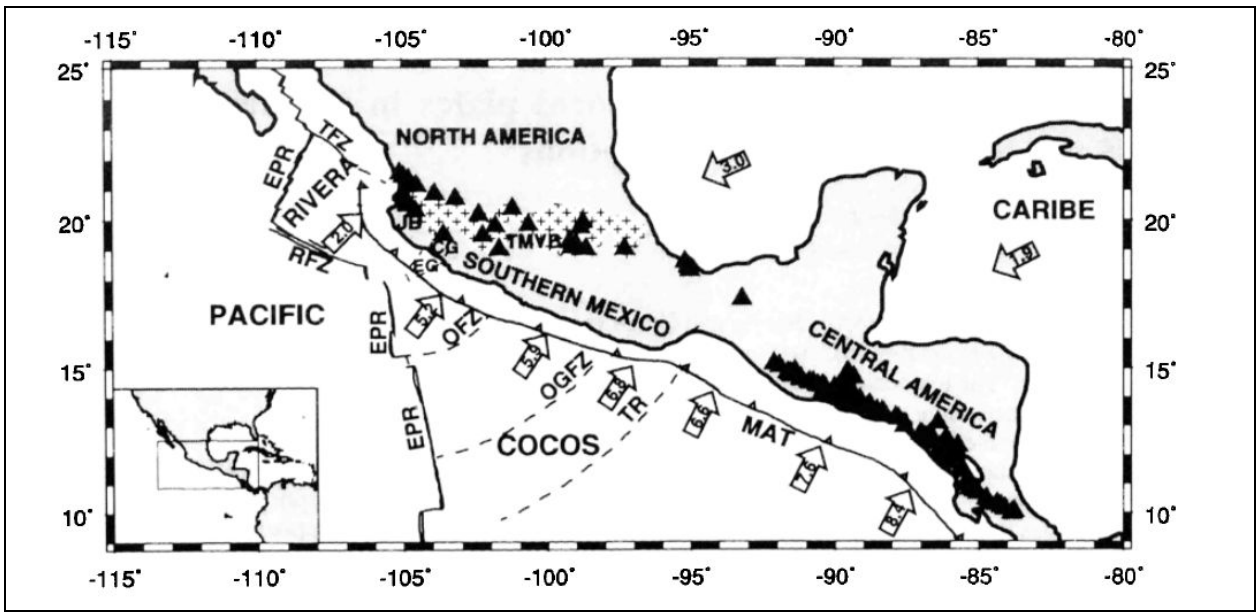

Figure 9. Cocos Subduction Zone - Pardo and Suarez, 1995.

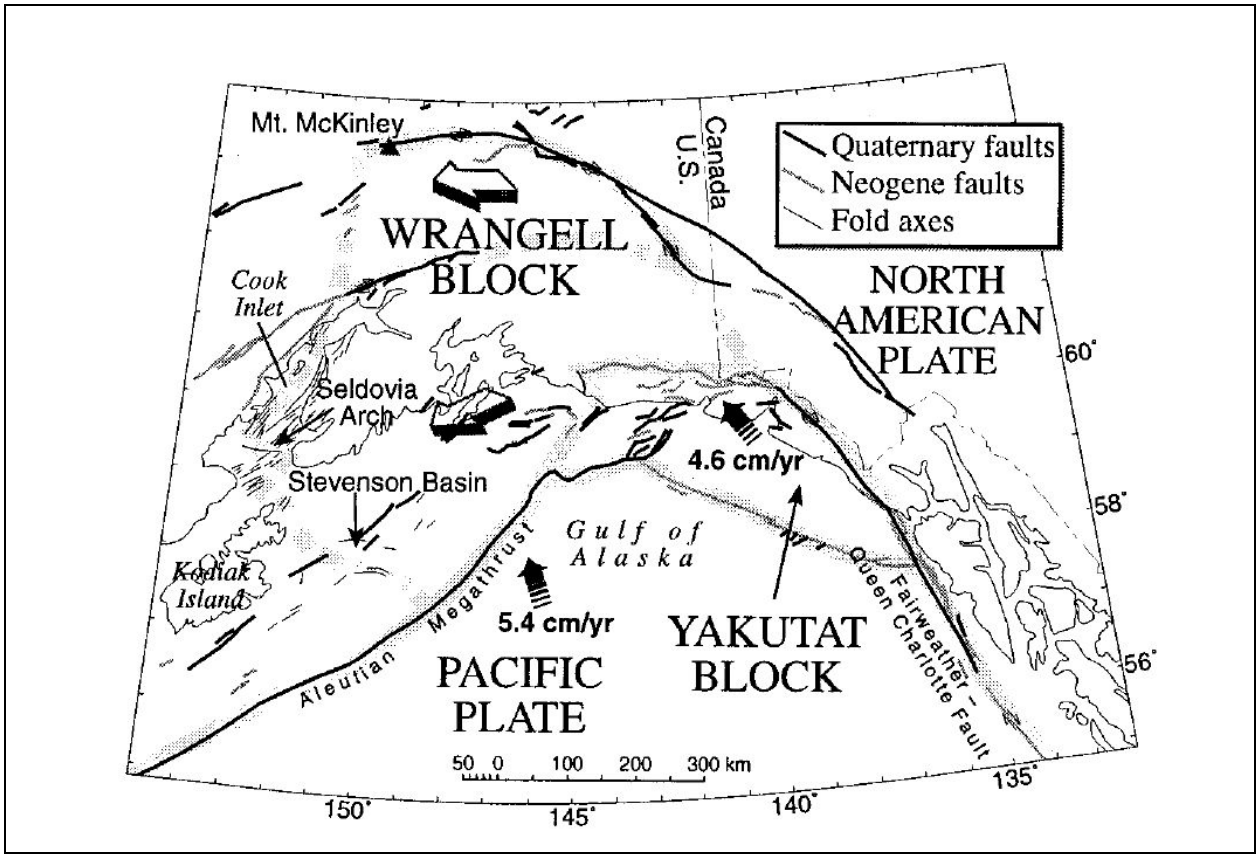

Figure 10. Tectonic setting for southern Alaska - Haessler et al., 2000.

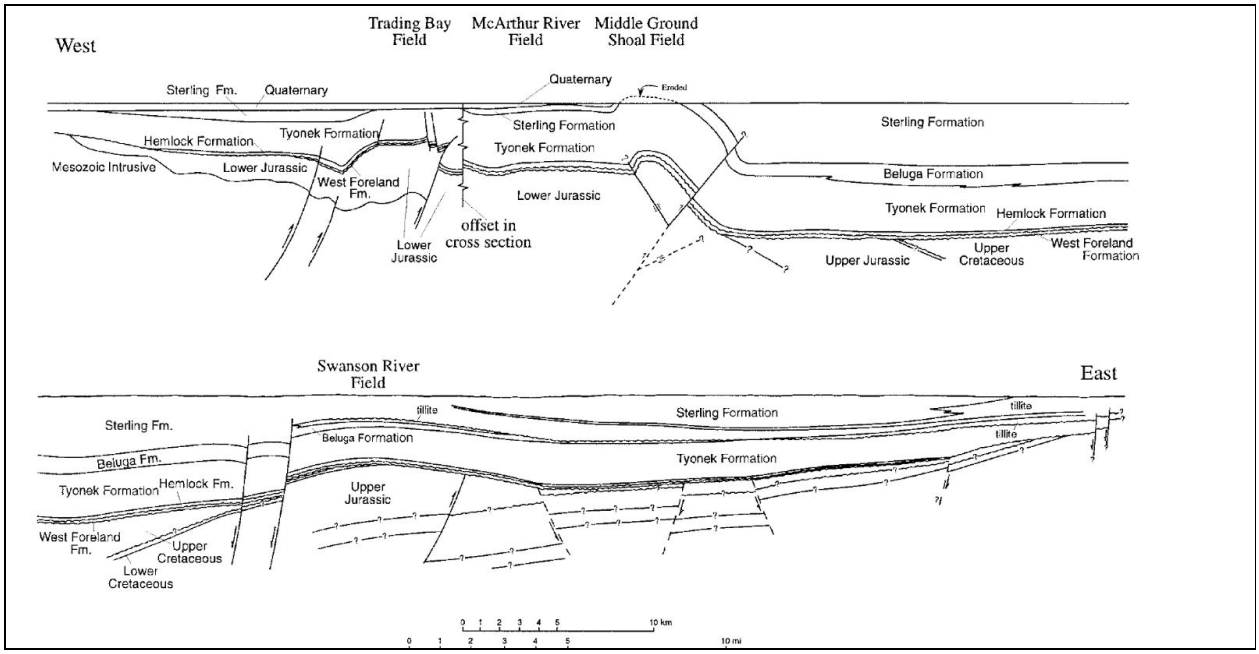

Figure 11. Cook Inlet Cross Section, Haeussler et al., 2000.

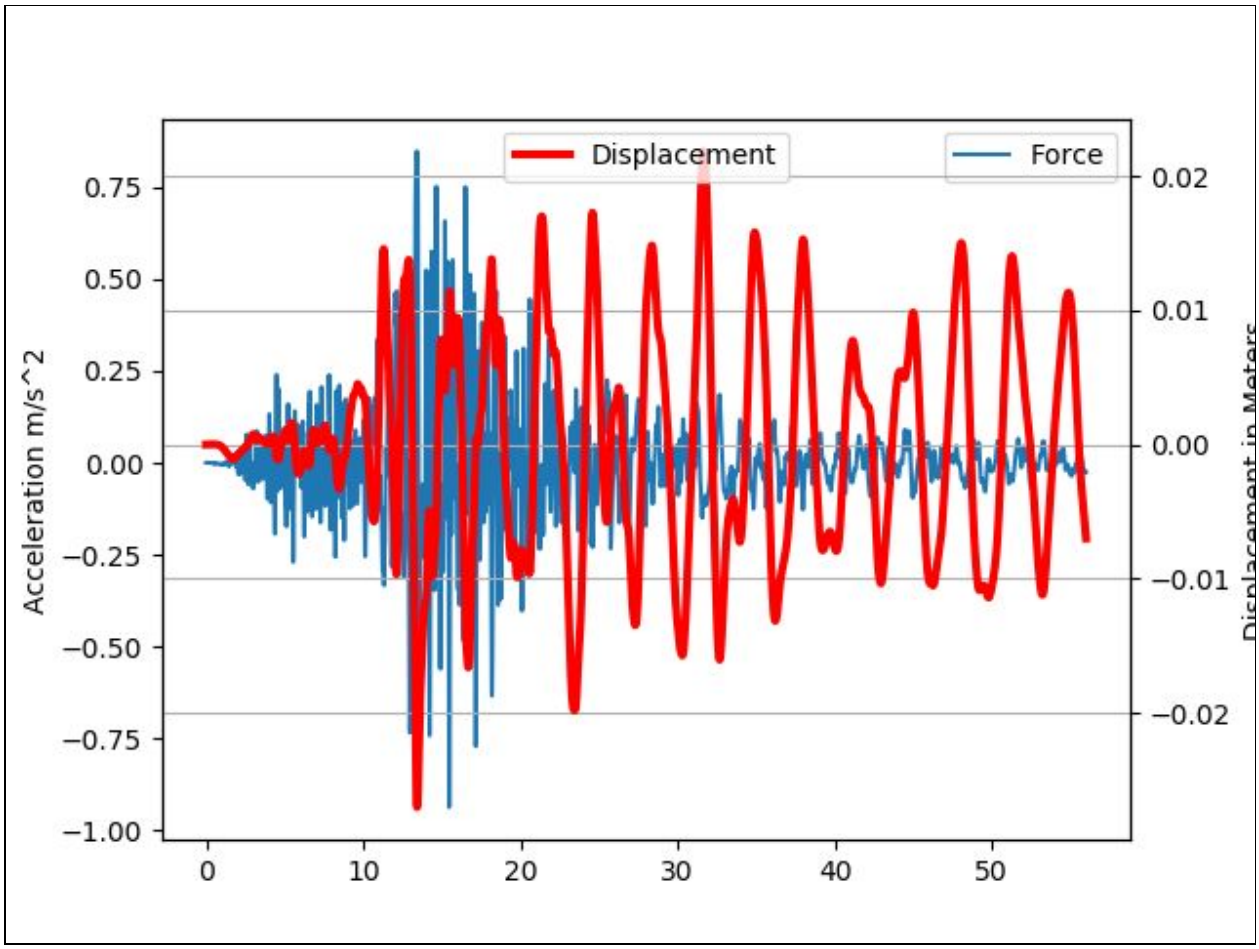

Figure 12. Six story building response from the 2001 Nisqually 6.8 magnitude earthquake at station HOLY. The x-axis is in seconds.

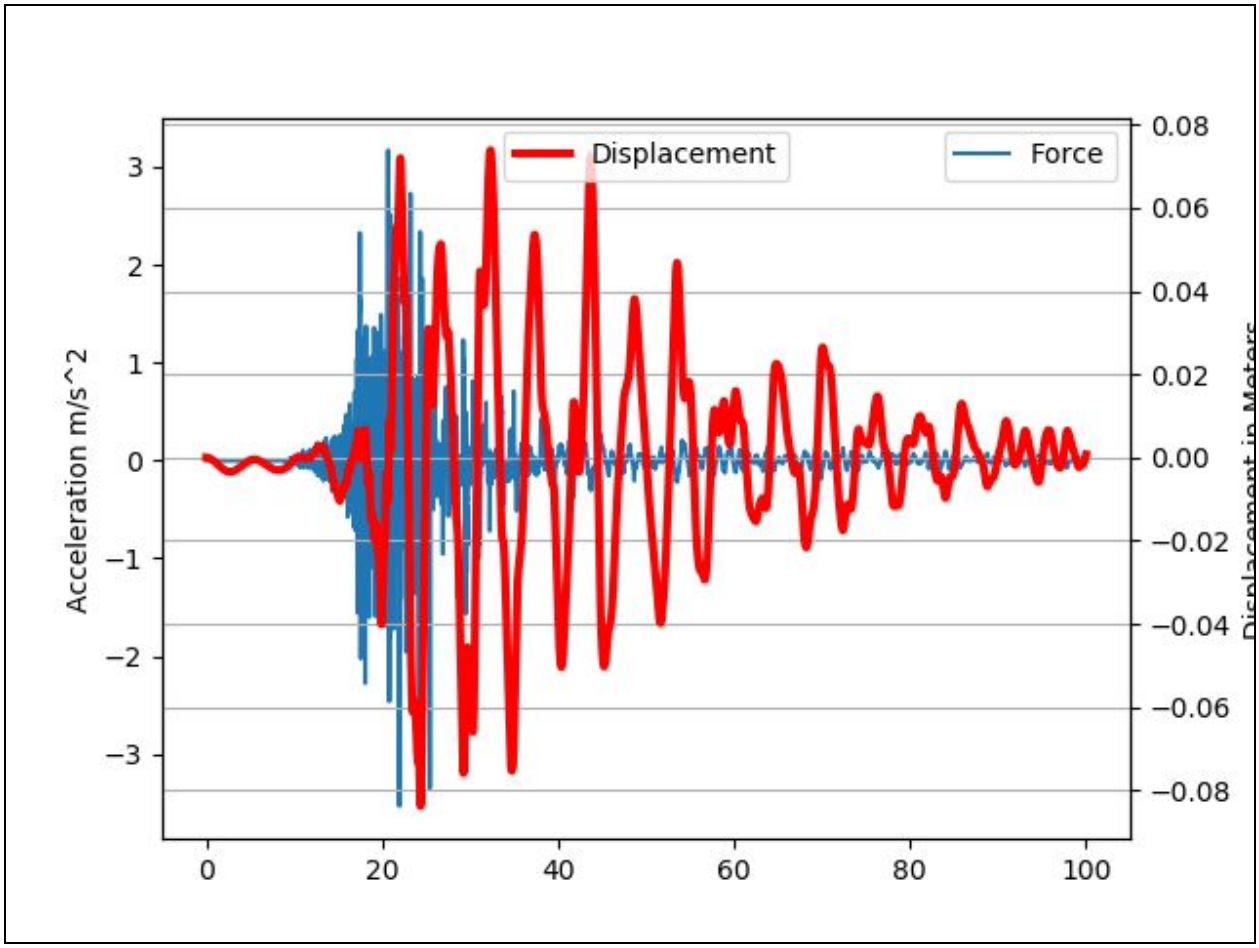

Figure 13. Sixteen story building response from the 2018 Anchorage 7.1 magnitude earthquake at station K211. X-axis is in seconds.

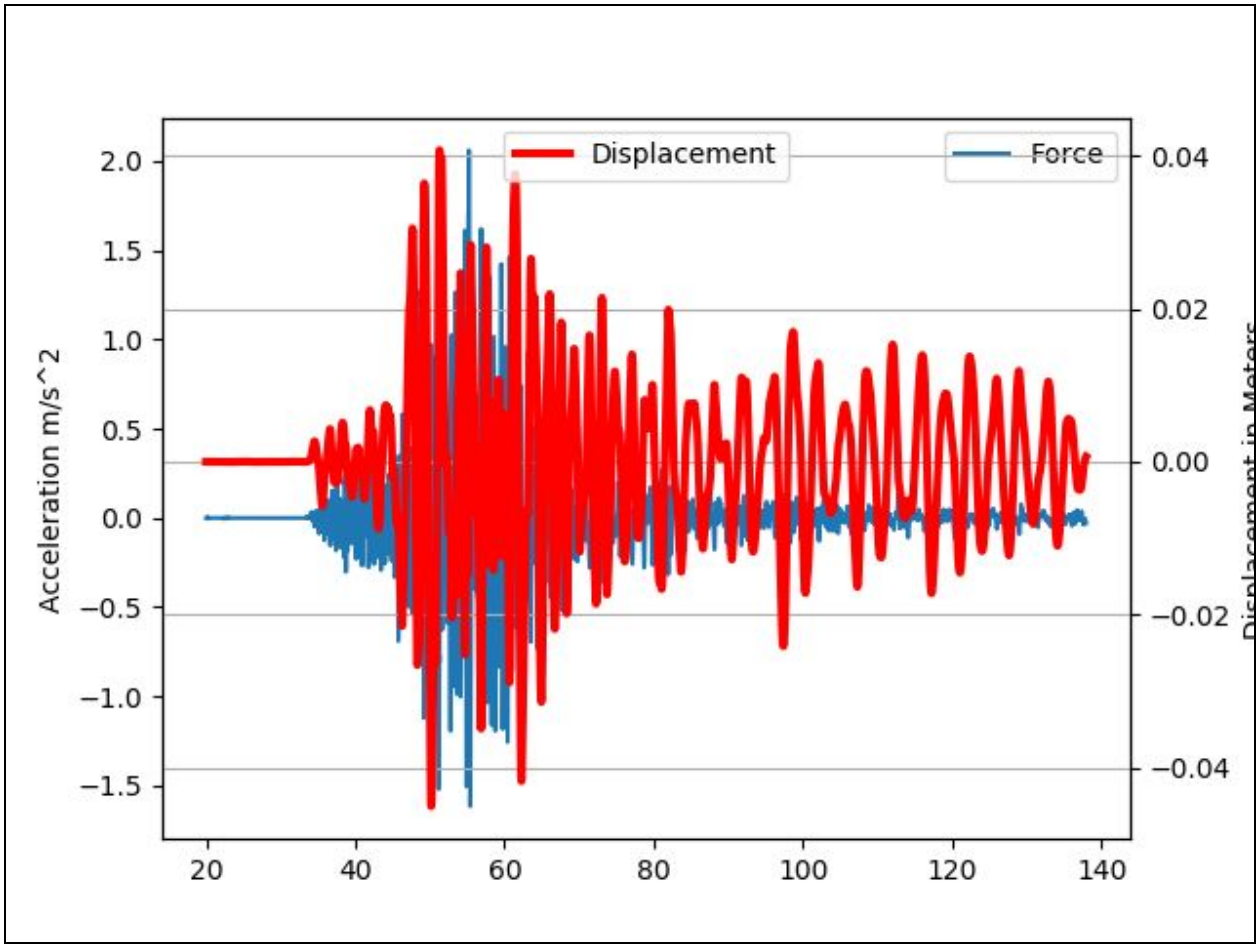

Figure 14. Six story building response from the 2017 7.1 magnitude Puebla Earthquake station MI15. X-axis is in seconds.

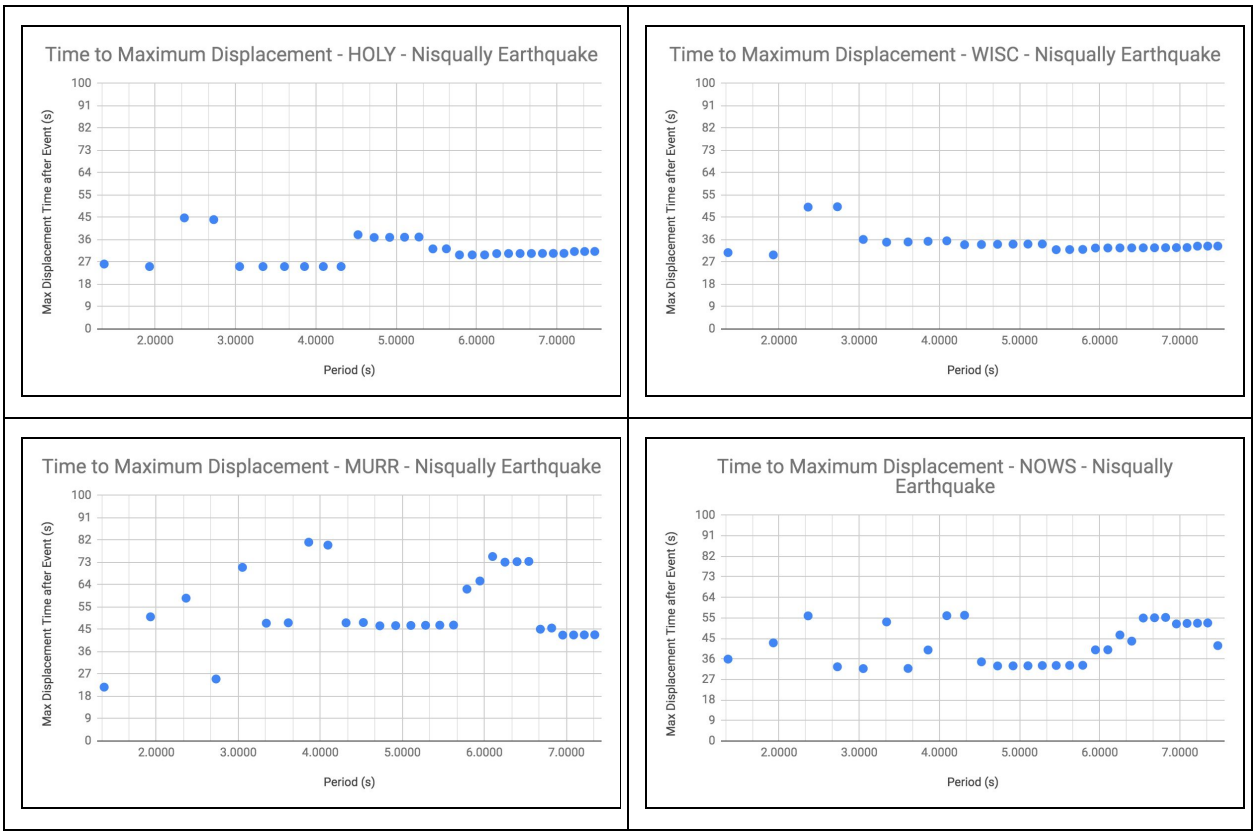

Figure 15. Maximum displacement times for different building periods during the Nisqually Earthquake. Stations are HOLY, 73 kilometers away from the hypocenter, WISC, 82 kilometers away, MURR, 58 kilometers away, and NOWS, 84 kilometers away. Smaller periods equate to shorter building heights while greater periods indicate taller buildings up to 30 stories high. Station MURR is closest to the rupture and appears more variation in timing of maximum displacement than others. This could be due to the local geology where there is undifferentiated Vashon drift. The site is no longer in existence.

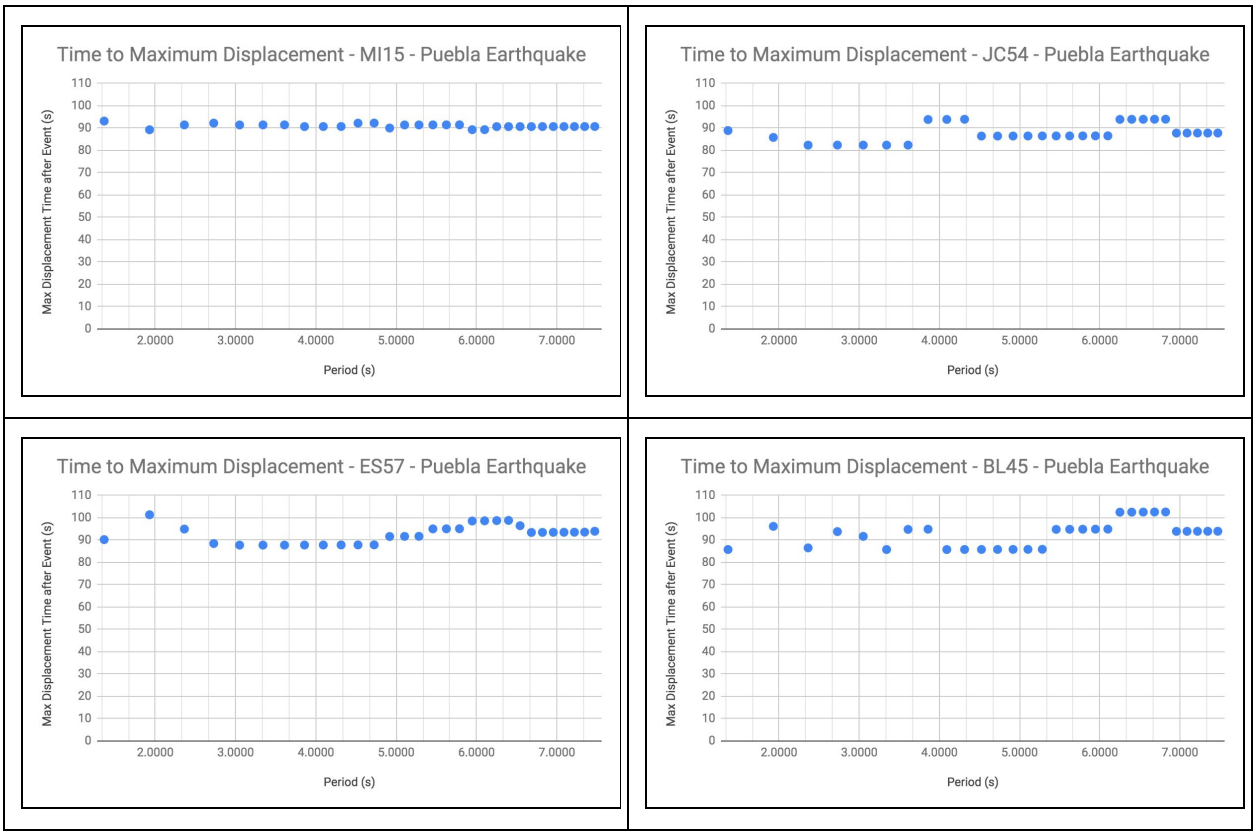

Figure 16. Maximum displacement times for different building periods during the Puebla earthquake. Stations are MI15, 116 kilometers away from the hypocenter, JC54, 120 kilometers away, ES57, 121 kilometers away, and BL45, 131 kilometers away. Smaller periods equate to shorter building heights while greater periods indicate taller buildings up to 30 stories high.

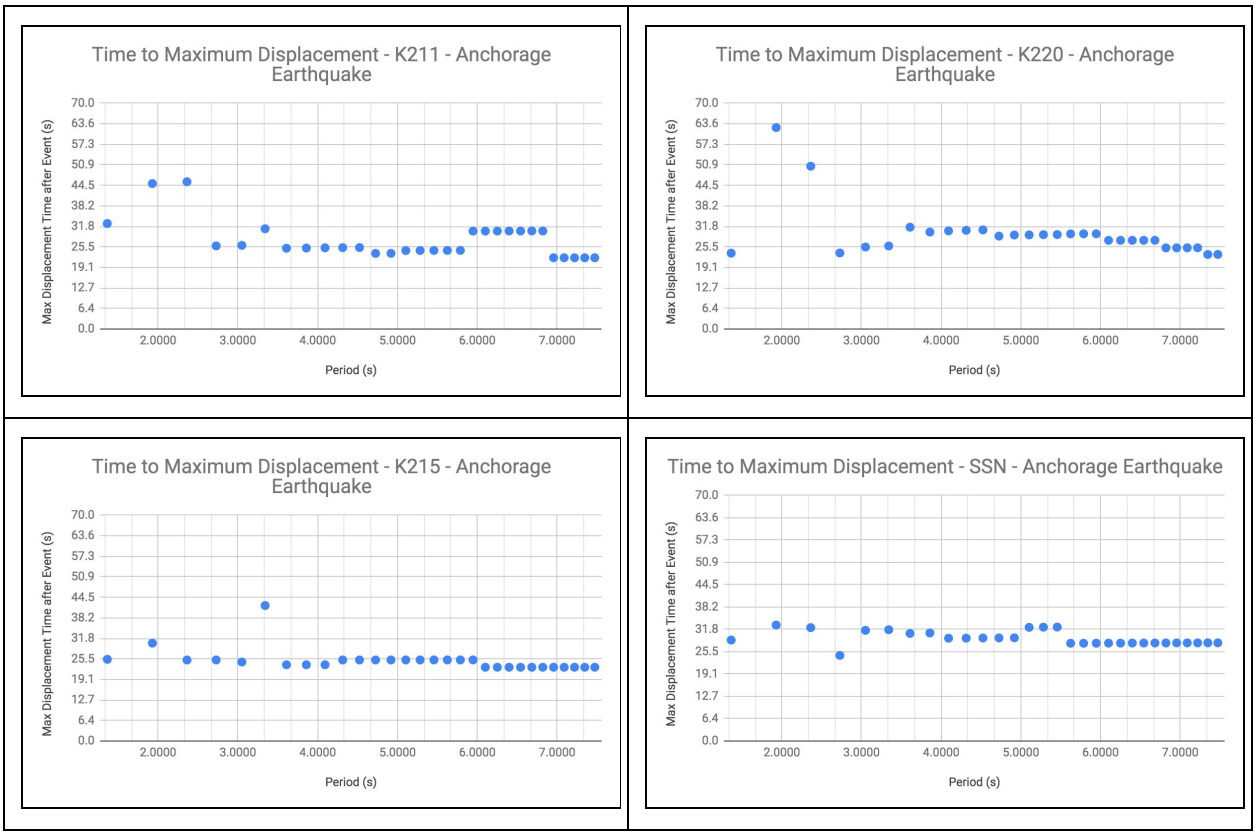

Figure 17. Maximum displacement times for different building periods during the Anchorage earthquake. Stations are K211, 52 kilometers away from the hypocenter, K220, 52 kilometers away, K215, 56 kilometers away, and SSN, 65 kilometers away. Smaller periods equate to shorter building heights while greater periods indicate taller buildings up to 30 stories high.

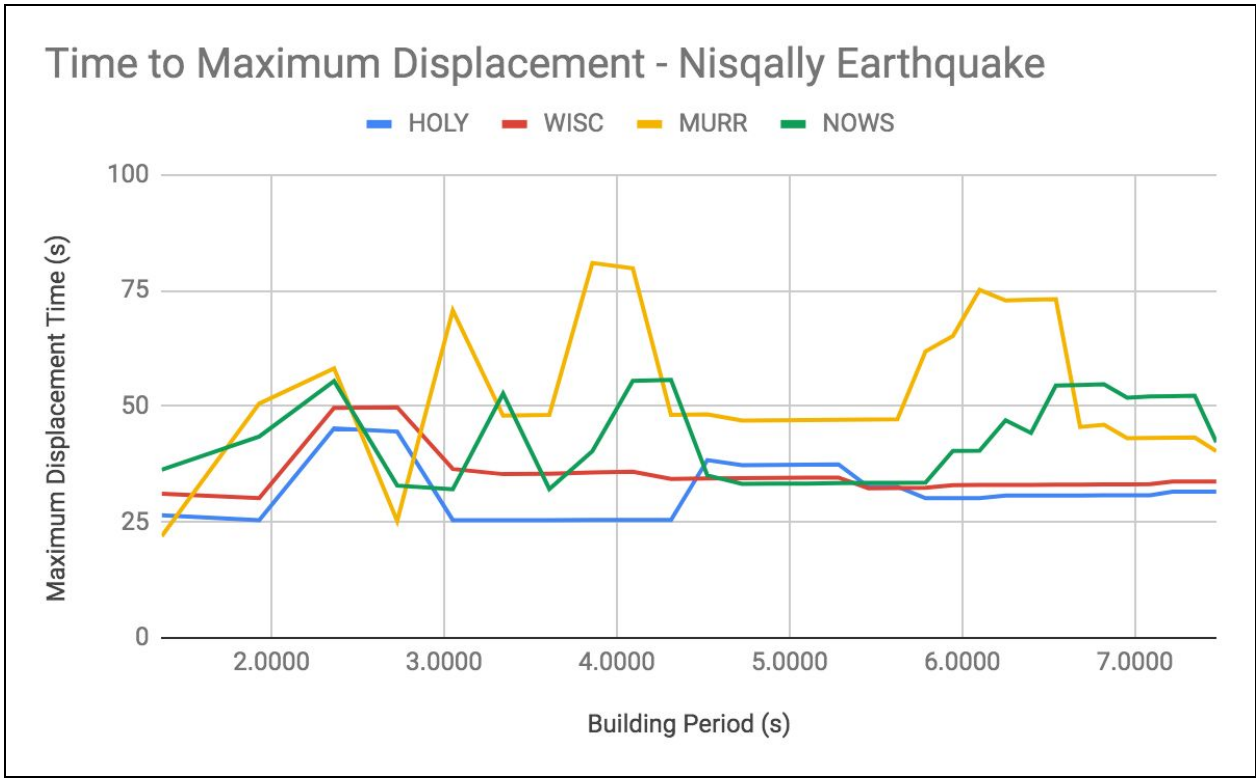

Figure 18. Building responses at Stations HOLY, WISC, MURR and NOWS for the Nisqually earthquake. Diagram is based off of scatter plots. The lines are meant as a visual aid and should not be inferred as a continuous representation of time.

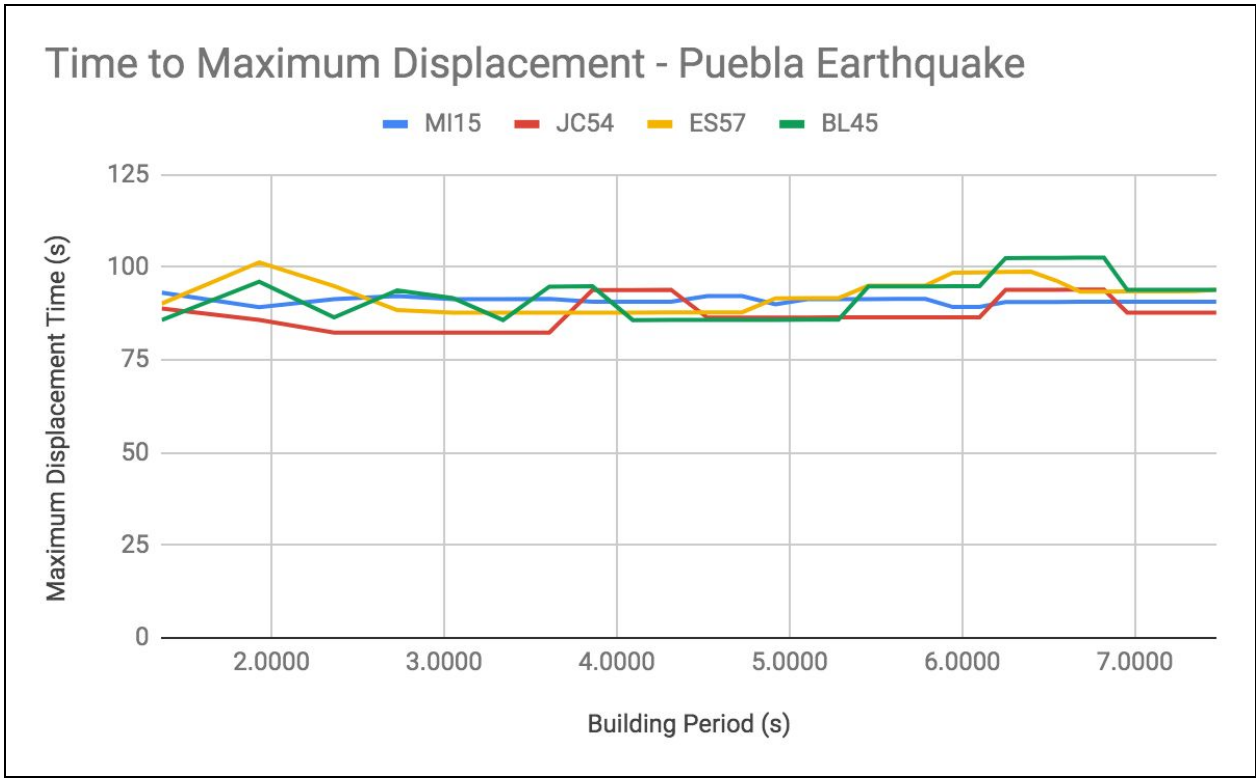

Figure 19. Building responses at Stations MI15, JC54, ES57 and BL45 for the Puebla earthquake. Diagram is based off of scatter plots. The lines are meant as a visual aid and should not be inferred as a continuous representation of time.

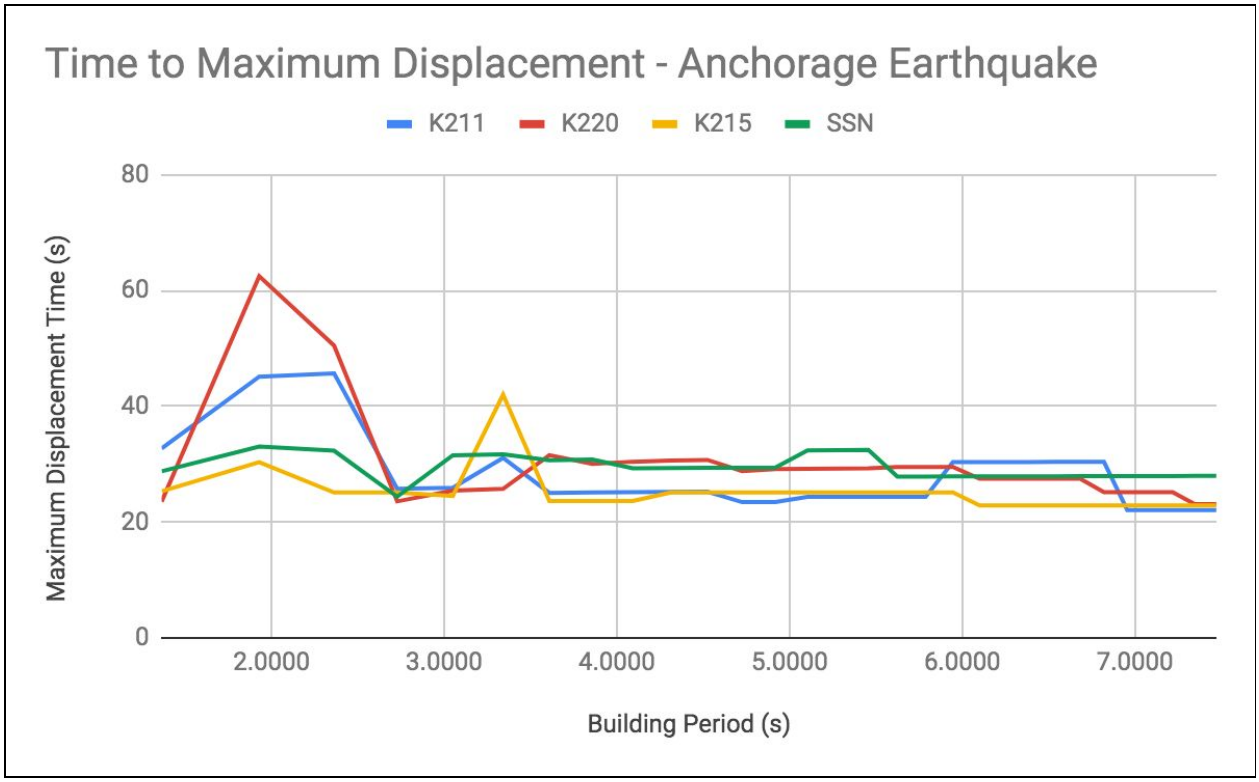

Figure 20. Building responses at Stations K211, K220, K215 and SSN for the Anchorage earthquake. Diagram is based off of scatter plots. The lines are meant as a visual aid and should not be inferred as a continuous representation of time.

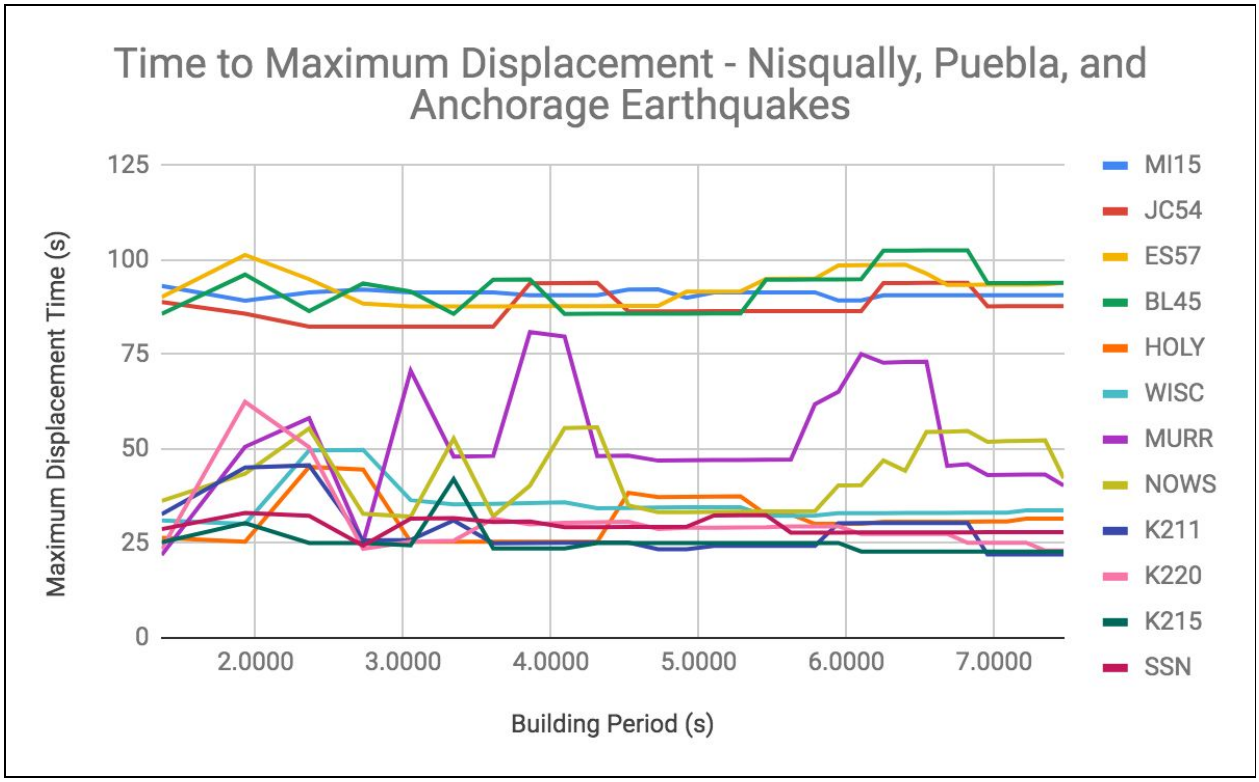

Figure 21. A comparison of all stations from each of the study areas. The lines are meant as a visual aid and should not be inferred as a continuous representation of time.

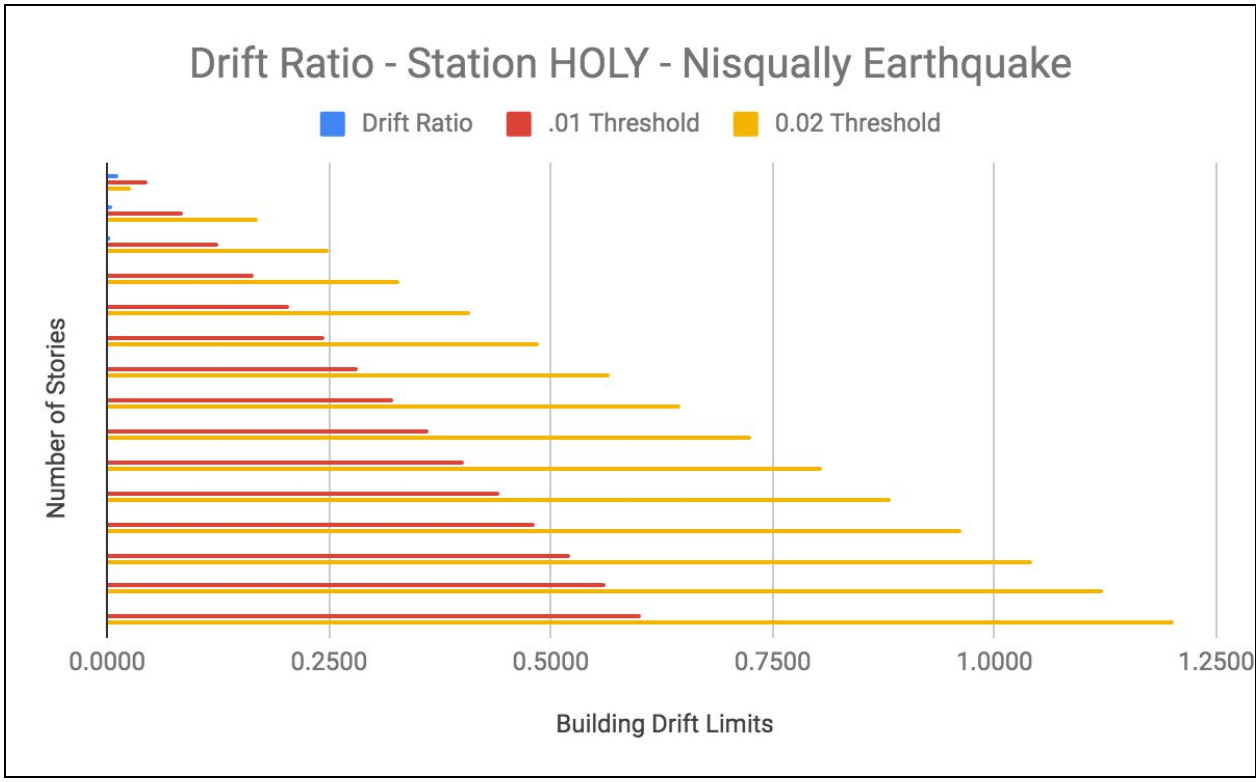

Figure 22. Drift ratio of building response - station HOLY - Nisqually earthquake.

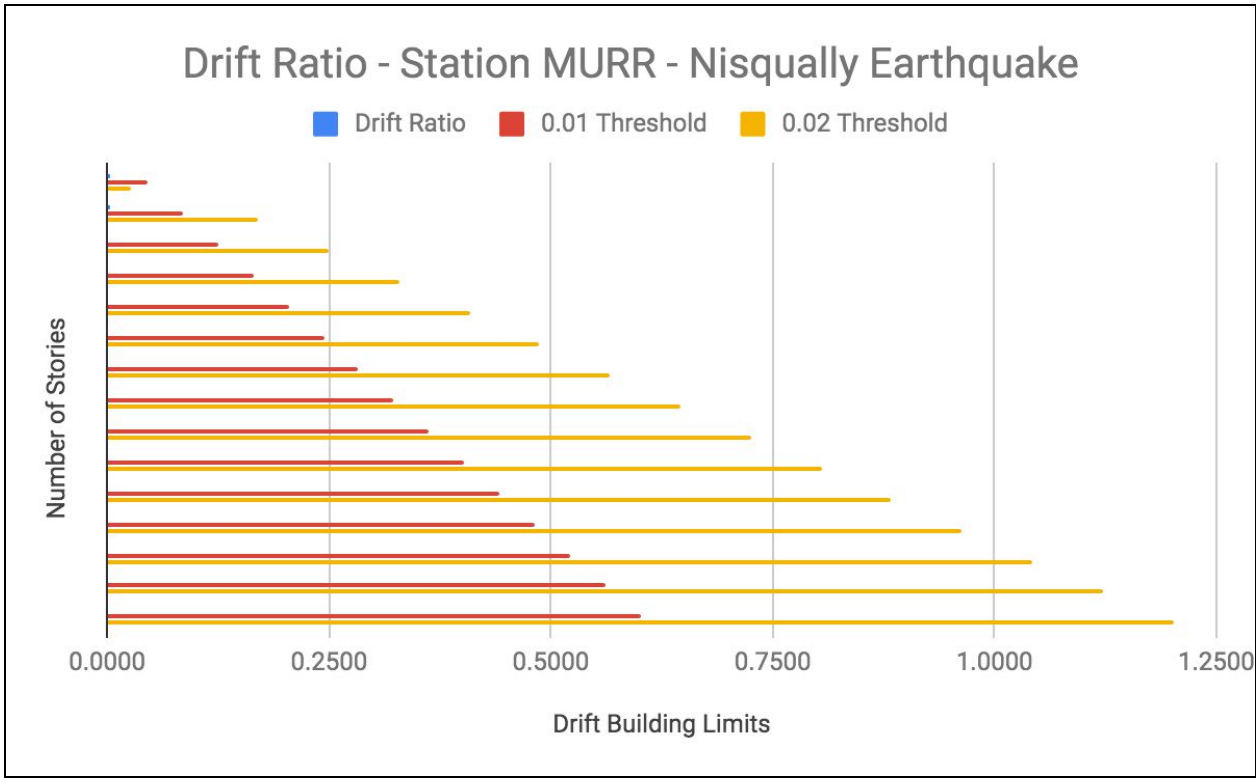

Figure 23. Drift ratio of building response - station MURR - Nisqually earthquake.

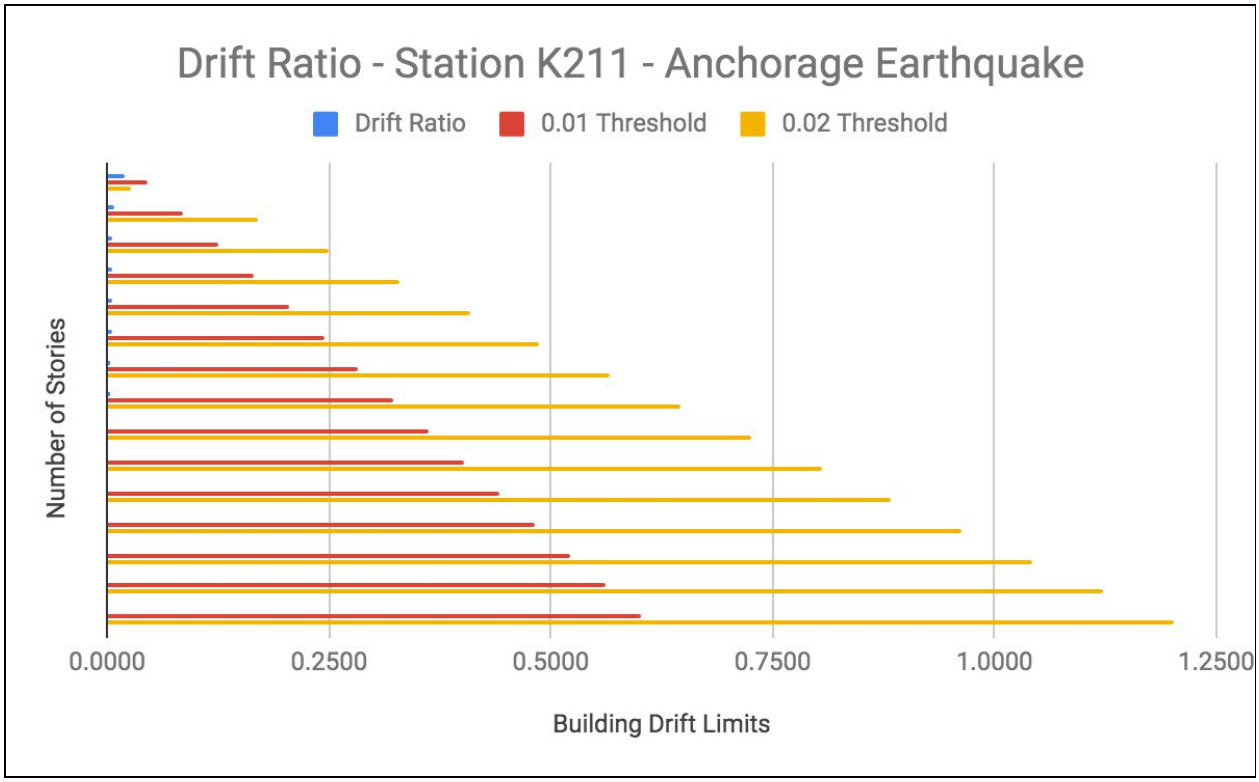

Figure 24. Drift ratio of building response - station K211 - Anchorage earthquake.

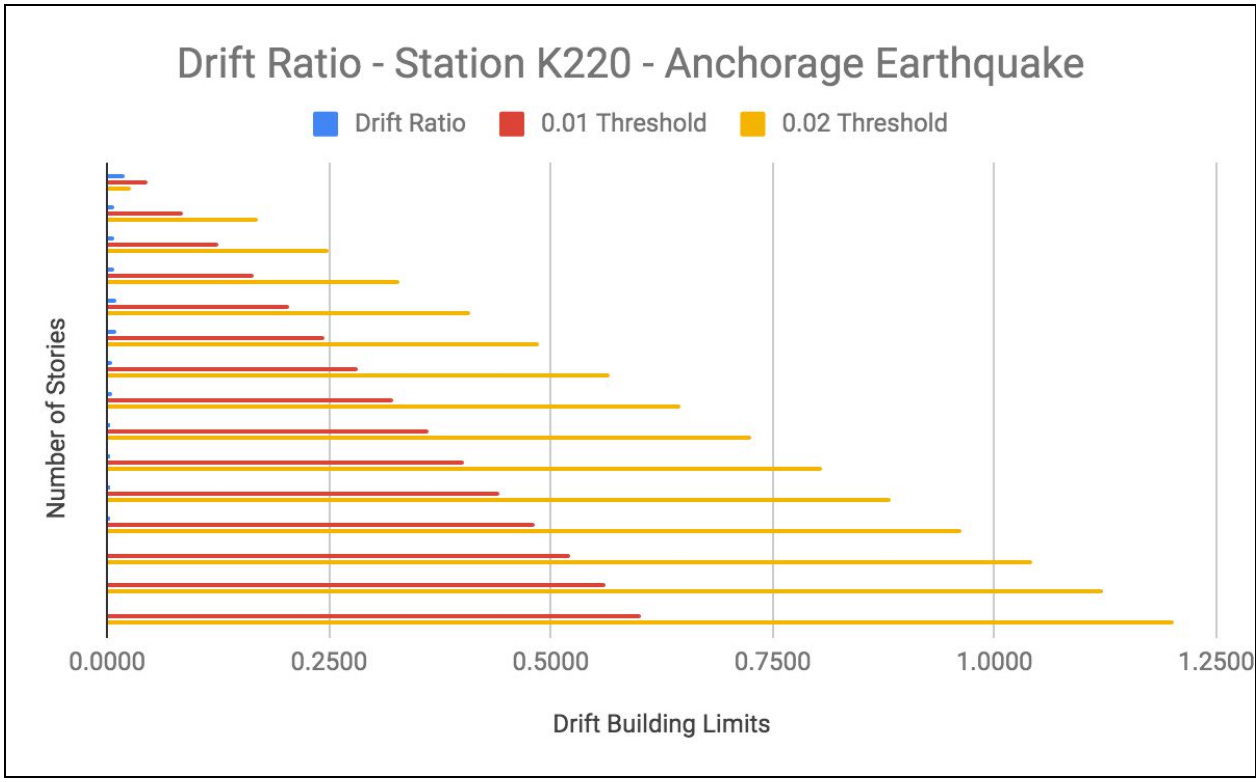

Figure 25. Drift ratio of building response - station K220 - Anchorage earthquake.

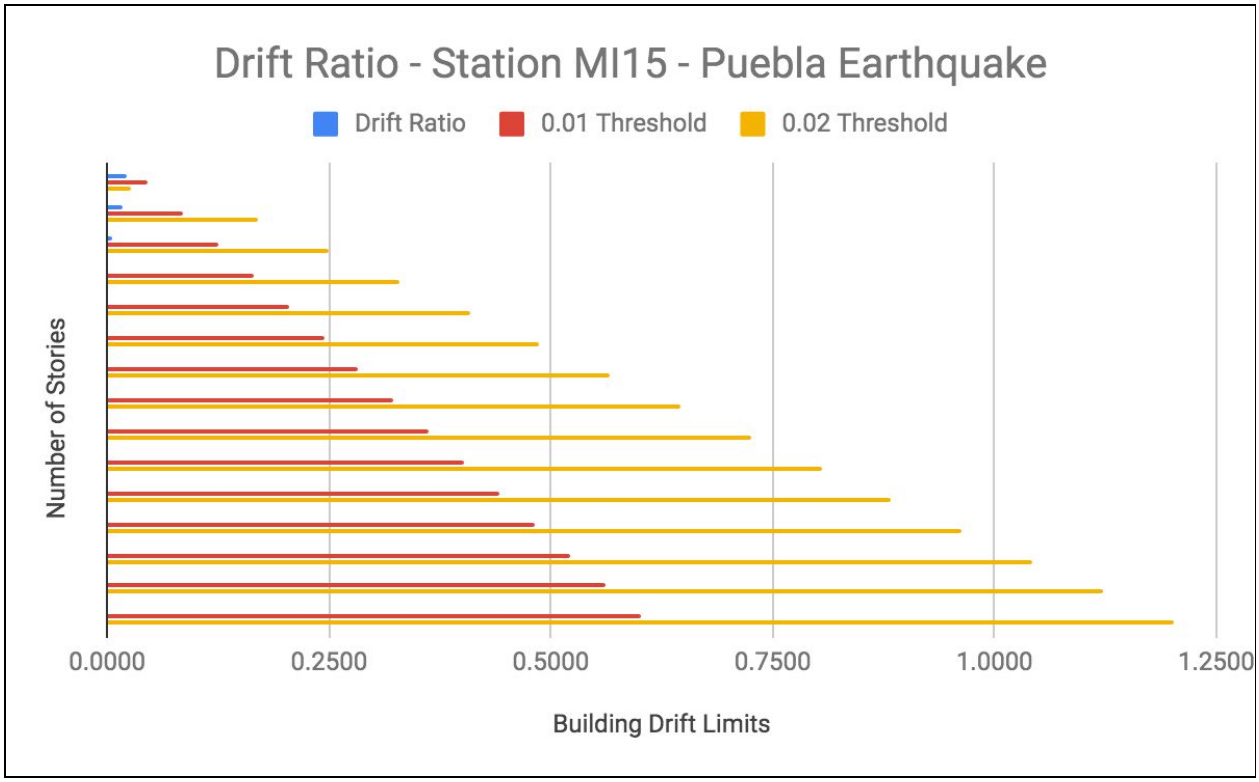

Figure 26. Drift ratio of building response - station MI15 - Puebla earthquake.

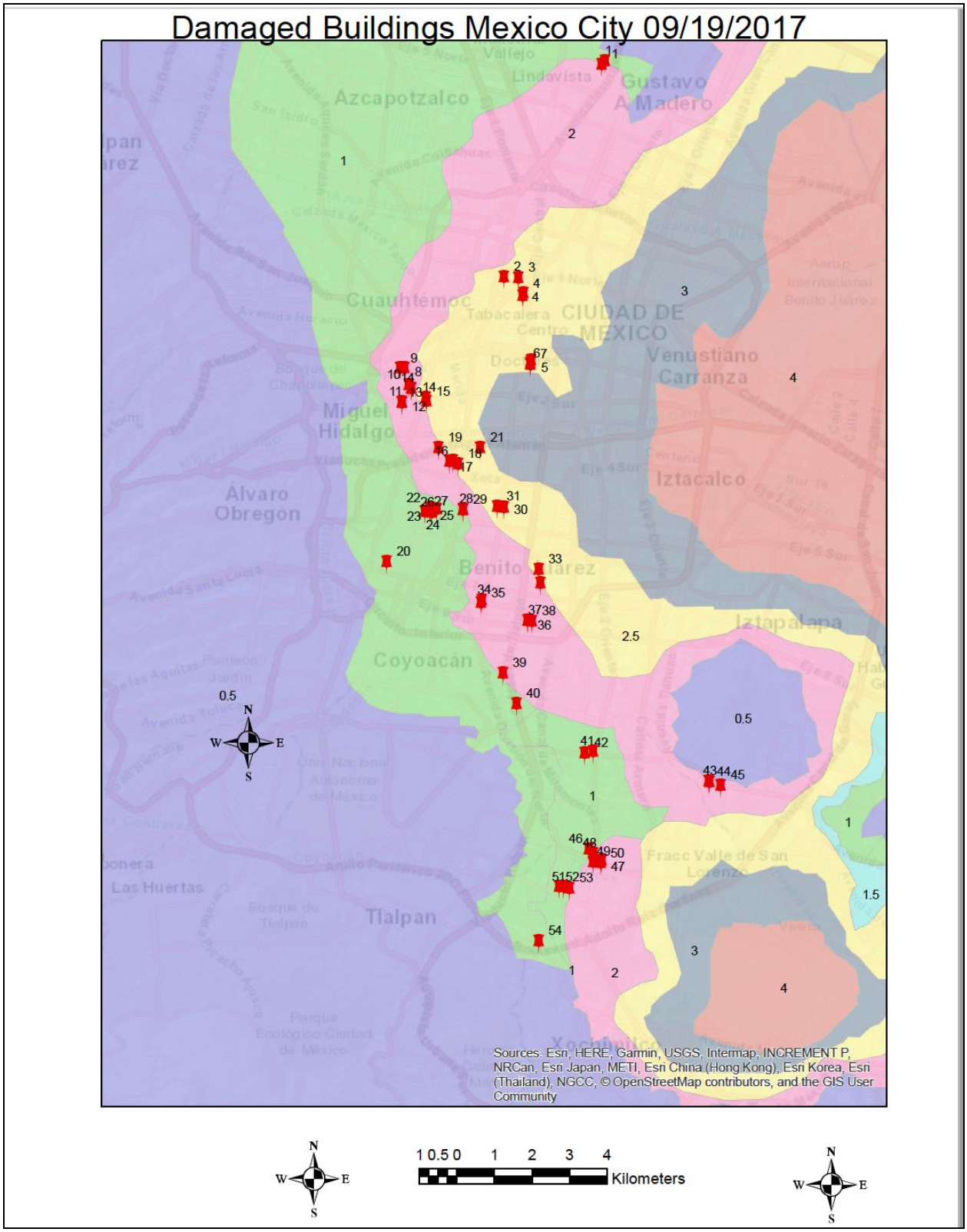

Figure 27. Map of the soil resonance periods in the Mexico City area with collapsed buildings in red.

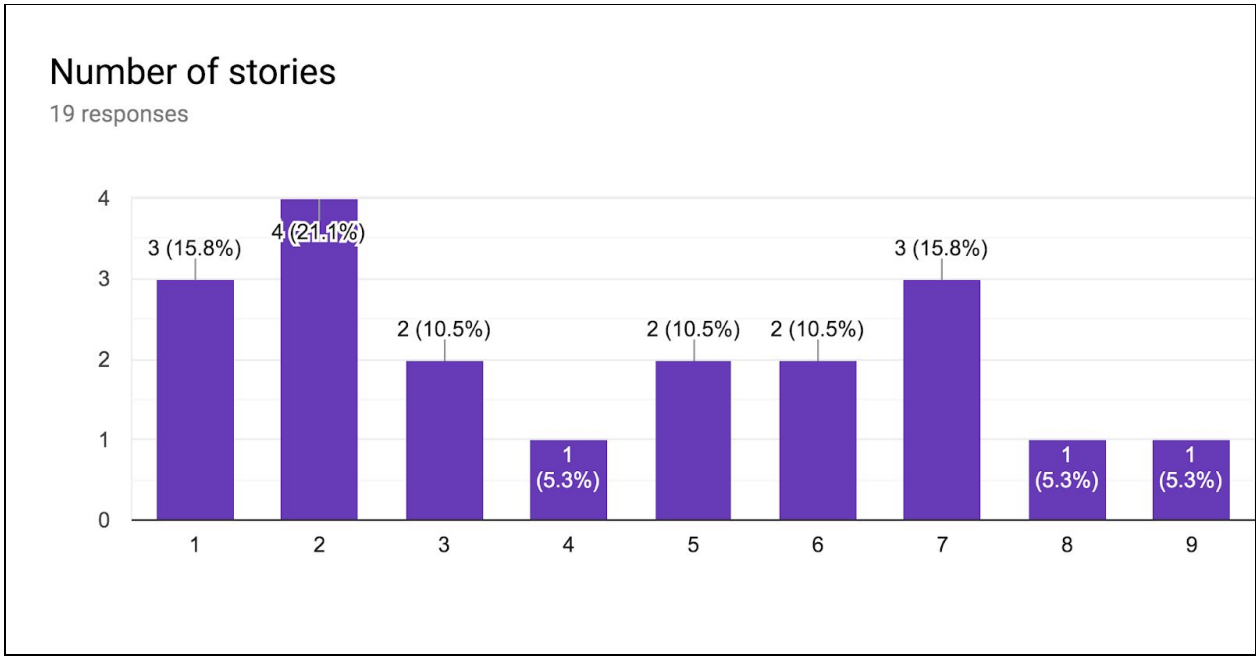

Figure 28. Chart from a Google Form for field survey in Mexico City. The x-axis represent the number of stories of a damaged building and the y-axis represents how many buildings were surveyed. In general buildings between 7 and 8 stories suffered damage in the 1 second period zone, 1 to 2 story tall buildings suffered damage in the 2.5 second period zone, 3 to 7 story buildings were damaged in the 2 second period zone, while a mixture of stories failed at the border between 1 to 2 second period seismic zones.

Appendix

1. Code for oscillator at github: https://github.com/nancysackman/oscillator
2. Link to google spreadsheet: sdofResultspython

OID	Ptype	Count	Group	Phi	C (psf)	unit weight (pcf)
0	Qal	35	Alluvium	30	50	120
	Qls		Landslide deposits	30	50	120
	Qmw		Colluvium	30	50	120
8	Qpfnc	3	Coarse-grained glacially consolidated deposits	36	100	130
10	Qpoc	10	Coarse-grained glacially consolidated deposits	36	100	130
13	Qpogc	3	Coarse-grained glacially consolidated deposits	36	100	130
17	Qponc	8	Coarse-grained glacially consolidated deposits	36	100	130
18	Qva	53	Coarse-grained glacially consolidated deposits	36	100	130
21	Qvr	49	Coarse-grained recessional outwash	34	50	130
1	Qf	5	Fan deposits	30	50	120
6	Qpff	12	Fine-grained glacially consolidated deposits	25	500	120
9	Qpfnf	12	Fine-grained glacially consolidated deposits	25	500	120
11	Qpof	7	Fine-grained glacially consolidated deposits	25	500	120
14	Qpogf	7	Fine-grained glacially consolidated deposits	25	500	120
20	Qvlc	16	Fine-grained glacially consolidated deposits	25	500	120
22	Qvrl	31	Fine-grained recessional outwash	20	250	115
23	Qvrlb	9	Fine-grained recessional outwash	20	250	115
24	Qvrlbt	3	Fine-grained recessional outwash	20	250	115
25	Qvrlf	8	Fine-grained recessional outwash	20	250	115
26	Qvrlj	13	Fine-grained recessional outwash	20	250	115
27	Qvrlo	3	Fine-grained recessional outwash	20	250	115
28	Qvrlr	5	Fine-grained recessional outwash	20	250	115
29	Qvrlt	10	Fine-grained recessional outwash	20	250	115
2	Ql	20	Lake deposits	20	150	110
3	Qob	5	Mixed glacially consolidated	30	250	125
5	Qpf	3	Mixed glacially consolidated deposits	30	250	125
7	Qpfn	12	Mixed glacially consolidated deposits	30	250	125
12	Qpog	5	Mixed glacially consolidated deposits	30	250	125
16	Qpon	9	Mixed glacially consolidated deposits	30	250	125
19	Qvi	15	Mixed glacially consolidated deposits	30	250	125
4	Qp	25	Peat and organic-rich deposits	24	50	70
31	Qw	5	Peat and organic-rich deposits	24	50	70
15	Qpogt	9	Till	38	500	145
30	Qvt	58	Till	38	500	145

Geology Summary Aug 23 2017

Table of Quaternary Deposits for the Puget Sound Basin

Field Observations in Mexico City

From March 25 to March 30, 2019, my colleague Mary Alice Benson and I traveled to Mexico City to survey a handful of buildings that failed or collapsed during the 2017 Puebla Earthquake. As mentioned previously in the background section, Mexico City sits on unconsolidated clay soils in the Valley of Mexico, a geologic basin surrounded by mountains and active volcanoes of the Trans Mexican Volcanic Belt. As a result of this geometry, Mexico City experiences devastating earthquakes that has caused buildings to collapse, both in the 1985 and 2017 earthquakes.

To optimize the time I had in Mexico City to survey the damaged buildings, I created a map in ArcGIS based on the seismic zones of the resonance periods of the soil there (Mexican Seismic Design Code, 2004). I then overlaid the building locations based on GPS points (source). I sampled a few building locations within each of the seismic zones (see figure 25).

My sampling strategy was to spend the least amount of time getting to a location. I chose our locations based on metro stops that would be in walking distance to the station. To minimize time taking notes, I created a Google form that could be used on my cell phone that would upload to a Google spreadsheet (see figure 26).

Examining the map, it should be noted that the .5 second resonance period indicates the bedrock or “rock” part of the city. Here, basalt outcrops in several areas of the city, including at UNAM and Tlalpan. The other resonance periods consist of alluvium and soft soils, mainly clay. Typically buildings are not damaged to failure in the .5 second seismic zone. Building failure for the 2017 Puebla Earthquake mainly occured in the 1 to 2.5 second resonance periods or seismic zones. During the survey of 18 structures, one to two story buildings typically failed in the 2.5 second zone. Three to seven story buildings failed in the 2 second zone. Seven to eight story buildings failed in the 1 second zone. And different ranges or mixed stories failed on the border between the 1 and 2 second zones.